CrystEngComm

PAPER

View Article Online
View Journal | View Issue

Check for updates

Cite this: *CrystEngComm*, 2024, **26**, 3574

Solvatomorphism with polar protic/aprotic and non-polar solvents in a series of complexes derived from the 5-phenylimidazole/tetrafluoroborate/copper(II) reaction system†

Maria-Ioanna Delegkou,[a] Nikos Panagiotou,[b] Constantina Papatriantafyllopoulou,[bc] Anastasios Tasiopoulos,[b] Dionissios Papaioannou,[a] Spyros P. Perlepes[a] and Vassilios Nastopoulos*[a]

In a search to explore the structural landscape of possible copper(II) complexes with the 4-phenylimidazole/ tetrafluoroborate combination, considerable solvatomorphism has emerged. The utilization of a wide variety of crystallization solvents (polar protic, polar and non-polar aprotic) resulted in a series of seventeen crystalline solvatomorphs with the general formulae $[Cu(BF_4)_2(HL)_4]\cdot x$(solvent) [HL = 5-phenylimidazole, *x*(solvent) = 2(acetone)·2(water) (**1**), 2(methanol) (**2**), 2(ethanol) (**3**), 2(1-propanol) (**4**), 1.4(2-propanol) (**5**), 2(1-butanol) (**6**), 2(iso-butanol) (**7**), 1.33(*tert*-butanol) (**8**), 2(1-pentanol) (**9**), 2(dimethylformamide) (**10**), 1.2(acetone) (**11**), 2(tetrahydrofurane) (**12**), 1.85(1,4-dioxane) (**13**), 0.86(ethyl acetate) (**14**), 1(diethyl ether) (**15**), 0.7(diisopropyl ether) (**16**), 1(*n*-hexane) (**17**)]. A reaction using the CH_2Cl_2/MeCN solvent system produced crystals of the $[Cu(HL)_4(MeCN)(H_2O)_{0.4}](BF_4)_2$ complex (**18**). Crystallization with nitromethane yielded $[Cu\{SiF_2O(OMe)\}_2(HL)_4]\cdot 0.8MeNO_2$ (**19**·$0.8MeNO_2$), due to the *in situ* reaction of fluoride ions from BF_4^- ions with the glass surface of the vial used to grow crystals. The structures have been solved by single-crystal X-ray diffraction and the complexes were characterized by thermal analysis and infrared spectroscopy. The crystallization solvents are located in channels, with the exception of 1.33(*tert*-butanol) (**8**) and 1.2(acetone) (**11**) residing in lattice pockets. An analysis to understand the role of the solvents in the molecular self-assembly process is described. Depending on the hydrogen-bond functionalities of each solvent, three distinct cases emerge i) the solvents link neighboring $[Cu(BF_4)_2(HL)_4]$ molecules *via* N–H···$O_{solvent}$–H···F intermolecular associations (polar protic solvents, compounds **1**–**9**), ii) they are terminally connected to $[Cu(BF_4)_2(HL)_4]$ molecules (polar aprotic solvents, compounds **10**–**13**) and iii) they simply reside in channels without any involvement in supramolecular motifs (non-polar solvents, compounds **14**–**17**). The final crystal packings result from the concerted action of robust N–H···F synthons and the above described interactions involving the solvent molecules.

Received 27th March 2024,
Accepted 31st May 2024

DOI: 10.1039/d4ce00304g

rsc.li/crystengcomm

Open Access Article. Published on 07 June 2024. Downloaded on 7/31/2025 6:43:31 AM.
This article is licensed under a Creative Commons Attribution 3.0 Unported Licence.

Introduction

Two important crystallization parameters are the solvent used and the environmental conditions during storage of the reaction solution (*e.g.* temperature, relative humidity).[1] Different solvents interact differently with a specific solute, affecting greatly the crystallization process.[2] The presence of guest lattice solvent molecules within the crystal can affect the molecular conformation of the host molecule in the structure, as well as the type and strength of intermolecular interactions that characterize the crystal lattice, resulting in different physicochemical properties, such as thermodynamic stability, density, solubility, dissolution rate.

Solvatomorphism, also named pseudopolymorphism, refers to the ability of a compound to yield crystal structures with unit cells that differ in their elemental composition through the inclusion of various amounts or types of solvent molecules,[3] or shortly, the term solvatomorphism is used for designating solvate diversity of a particular host compound.[4] There has been a long discussion and interesting arguments among experts in the field on the use of the terms solvatomorph and pseudopolymorph (or supramolecular

[a] *Department of Chemistry, University of Patras, 26504 Patras, Greece. E-mail: nastopoulos@upatras.gr*
[b] *Department of Chemistry, University of Cyprus, 1678 Nicosia, Cyprus*
[c] *National University of Ireland Galway, H91 TK 33 Galway, Ireland*

† Electronic supplementary information (ESI) available: CCDC 2342307–2342325. For ESI and crystallographic data in CIF or other electronic format see DOI: https://doi.org/10.1039/d4ce00304g

This journal is © The Royal Society of Chemistry 2024

Open Access Article. Published on 07 June 2024. Downloaded on 7/31/2025 6:43:31 AM.
This article is licensed under a Creative Commons Attribution 3.0 Unported Licence.

isomer, co-crystal, solvate, or even false polymorph or quasipolymorph) that could describe, as clear and concise as possible, the above category of crystalline structures.[5–13] Reaching consensus on this issue is important for scientific communication, and possibly also for intellectual property purposes.[14] In the current study we opted for the term solvatomorphism, to point out that the crystalline structures $[Cu(BF_4)_2(HL)_4]\cdot x$(solvent) presented here, where HL is 5-phenylimidazole, differ in the type of *solvent* incorporated during crystallization of the molecule. Polymorphism (the phenomenon wherein the same substance exhibits different crystal packing arrangements[15]) and solvatomorphism have been interesting topics in crystal *structure* engineering in relation to the implications on the crystal packing (structural patterns, pre-desired topologies) and, ultimately, to the potential impact on the properties of crystalline solids (crystal *property* engineering).[16–18] With respect to solvatomorphism in particular, the effect of the solvent on the organization of the supramolecular systems (based on solute-solvent specific interactions) is well-known and of great interest, both for academic studies and practical applications.[19–21] For example, this has implications in pharmaceutical compounds (affecting their bioavailability, stability, purification process, among other factors, and hence the performance of the drug), in biological systems (where denaturation of proteins, by altering the protein solvent environment, results in significant changes in their biological activities), in the material sciences (*e.g.* in the self-assembly of MOFs,[22,23] in organic and inorganic functional nanomaterials,[24,25]) to cite a few areas. It is noted that for some important compounds, such as active pharmaceutical ingredients (APIs), solvatomorphs are the only kind of crystalline forms available for use in single-crystal X-ray diffraction studies.

Over the last years we have prepared and studied a series of 3d metal complexes with substituted imidazole ligands to identify the trends and patterns upon which their molecular and supramolecular assembly is organized, particularly with respect to intermolecular hydrogen-bond motifs and other weak interactions.[26–31] With respect to this, we directed the present study to the use of the relatively small and flexible 4-phenylimidazole ligand (HL, Scheme 1) in combination with the tetrafluoroborate salt of copper(II). Copper(II) is an interesting and popular metal ion in coordination chemistry and has been named 'chameleon'[32] as it favours a variety of coordination numbers and geometries[33] that can be realized by properly selecting the ligands and the reaction conditions. The $3d^9$ configuration makes copper(II) subject to Jahn–Teller distortion and this plays a predominant role in its stereochemistry. Thus, square planar or distorted tetrahedral (4-coordinate), square pyramidal or trigonal bipyramidal (5-coordinate), as well as distorted octahedral (6-coordinate) geometries dominate the coordination chemistry of copper(II). Imidazole and its derivatives[34,35] are, among others, particularly interesting ligands in bioinorganic[36,37] and metallosupramolecular chemistry, employed, for example, in the synthesis of clusters, coordination polymers and MOFs.[38,39] 4-phenylimidazole can coordinate to a metal ion *via* its pyridine-type N3-atom towards mononuclear species. At the supramolecular level, the ligand has a hydrogen-bond donor (the pyrrolic-type N1-atom) enabling the formation of strong motifs[38,40–43] and is also capable of forming π···π stackings[44–46] through its 5- and 6-membered aromatic rings.

The tetrafluoroborate ion usually acts as a counter-ion in coordination compounds. Due to its small size, non-nucleophilicity, resistance to coordination and stability, the BF_4^- ion finds extensive uses as the anion in ionic liquids, as a substitute for ClO_4^- ion that forms explosive salts, as a spectator for chelates of catalytic transition metals (*e.g.* Au,

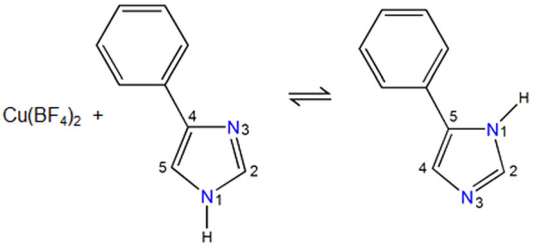

solvent used		
Polar protic solvents	$[Cu(BF_4)_2(HL)_4]\cdot 2Me_2CO\cdot 2H_2O$	**1**·$2Me_2CO\cdot 2H_2O$
	$[Cu(BF_4)_2(HL)_4]\cdot 2MeOH$	**2**·2MeOH
	$[Cu(BF_4)_2(HL)_4]\cdot 2EtOH$	**3**·2EtOH
	$[Cu(BF_4)_2(HL)_4]\cdot 2$(1-PrOH)	**4**·2(1-PrOH)
	$[Cu(BF_4)_2(HL)_4]\cdot 1.4$(2-PrOH)	**5**·1.4(2-PrOH)
	$[Cu(BF_4)_2(HL)_4]\cdot 2$(1-BuOH)	**6**·2(1-BuOH)
	$[Cu(BF_4)_2(HL)_4]\cdot 2$(*iso*-BuOH)	**7**·2(*iso*-BuOH)
	$[Cu(BF_4)_2(HL)_4]\cdot 1.33$(*tert*-BuOH)	**8**·1.33(*tert*-BuOH)
	$[Cu(BF_4)_2(HL)_4]\cdot 2$(1-PeOH)	**9**·2(1-PeOH)
Polar aprotic solvents	$[Cu(BF_4)_2(HL)_4]\cdot 2DMF$	**10**·2DMF
	$[Cu(BF_4)_2(HL)_4]\cdot Me_2CO$	**11**·$1.2Me_2CO$
	$[Cu(BF_4)_2(HL)_4]\cdot 2THF$	**12**·2THF
	$[Cu(BF_4)_2(HL)_4]\cdot 1.85$(1,4-dioxane)	**13**·1.85(1,4-dioxane)
Non-polar solvents	$[Cu(BF_4)_2(HL)_4]\cdot 0.86EtOAc$	**14**·0.86EtOAc
	$[Cu(BF_4)_2(HL)_4]\cdot Et_2O$	**15**·Et_2O
	$[Cu(BF_4)_2(HL)_4]\cdot 0.7DIPE$	**16**·0.7DIPE
	$[Cu(BF_4)_2(HL)_4]\cdot$(*n*-hexane)	**17**·(*n*-hexane)
CH_2Cl_2/MeCN	$[Cu(HL)_4(MeCN)(H_2O)_{0.4}](BF_4)_2$	**18**
$MeNO_2$	$[Cu\{SiF_2O(OMe)\}_2(HL)_4]\cdot 0.8MeNO_2$	**19**·$0.8MeNO_2$

Scheme 1 The general synthetic route and the crystallographically determined formulae of the Cu(II) complexes with 5-phenylimidazole (HL) as ligand. The initially used 4-phenylimidazole ligand is present in all complexes as its 5-phenylimidazole tautomeric form.

Open Access Article. Published on 07 June 2024. Downloaded on 7/31/2025 6:43:31 AM. This article is licensed under a Creative Commons Attribution 3.0 Unported Licence.

Pd, Pt) and as a counter-ion to highly reactive cations, such as nitrosonium, nitronium, pyrylium, aryldiazonium, triethoxonium (in Meerwein's salt) and iodonium (in Barluenga's reagent).[47] During the last 40 years or so, there have been reports showing that the BF_4^- ion is not always stable, and that reaction with the ligand or the metal ion in coordination complexes may occur, often resulting in F^--containing compounds.[48,49] Another interesting aspect of the chemistry of BF_4^- is that sometimes it can coordinate to metal ions in a terminal (monodentate) or bridging manner, but seldom coordination is strong.[50–52] We have, therefore, chosen as a source of copper(II) the $Cu(BF_4)_2{\cdot}6H_2O$ salt in order to study the tetrafluoroborate coordination ability and provide the copper(II) ion with the conditions to realize the optimal coordination geometry from the 5-phenylimidazole/tetrafluoroborate ligand system available.

Following this approach, we have prepared and characterized a total of nineteen new Cu(II) complexes (Scheme 1). Notable solvatomorphism was observed among them and, utilizing a variety of crystallization solvents, seventeen of these compounds (**1**–**17**) were found to be solvatomorphs with the general formula $[Cu(BF_4)_2(HL)_4]{\cdot}x$(solvent). Alongside, compounds $[Cu(HL)_4(MeCN)(H_2O)_{0.4}](BF_4)_2$ (**18**) and $[Cu\{SiF_2O(OMe)\}_2(HL)_4]{\cdot}0.8MeNO_2$ (**19**·0.8$MeNO_2$) were also isolated and characterized (see below). All structures (molecular and supramolecular) have been studied and compared to explore the role of the solvent molecules (in terms of hydrogen-bonding capacity, size, shape) in the solvatomorph self-assembly process in the solid state.

Experimental

Materials and instruments

All reagents and starting materials were reagent grade, purchased from standard suppliers and used as received. All manipulations were performed under aerobic conditions. Microanalyses (C, H, N) were performed by the University of Patras microanalytical service. IR spectra (4000–400 cm^{-1}) were recorded on a Perkin-Elmer PC 16 FT-IR spectrometer with the samples prepared as KBr pellets. Thermal decomposition measurements for selected complexes were performed using a Shimadzu TGA 50 analyzer under air; the rate of the temperature increase was 10 °C min^{-1}.

Preparation of complexes

Synthesis of $[Cu(BF_4)_2(HL)_4]{\cdot}2Me_2CO{\cdot}2H_2O$ (1·2Me_2CO·2H_2O). Solid $Cu(BF_4)_2{\cdot}6H_2O$ (0.138 g, 0.40 mmol) was added under stirring to a solution of HL (0.144 g, 1.00 mmol) in Me_2CO (25 mL). The resultant green solution was stirred for 30 min, then filtered and the mauve filtrate was layered with *n*-hexane (5 mL/5 mL). Pale purple crystals of **1**·2Me_2CO·2H_2O were obtained after eight days, they were collected by filtration, washed with Et_2O (2 × 5 mL) and dried *in vacuo*. Yield *ca.* 65% (based on HL). Anal. calcd for **1**·2H_2O (found values in parentheses): C 50.88 (51.21), H 4.27 (4.13), N 13.18 (13.44)%. Selected IR bands (KBr, cm^{-1}): 3410sb, 3152m, 1676m, 1491m, 1172m, 1118s, 1076s, 1035s, 941m, 757s, 689m, 644m, 513m.

Synthesis of $[Cu(BF_4)_2(HL)_4]{\cdot}2MeOH$ (2·2MeOH). Solid $Cu(BF_4)_2{\cdot}6H_2O$ (0.086 g, 0.25 mmol) was added under stirring to a solution of HL (0.144 g, 1.00 mmol) in MeOH (25 mL). The resultant blue solution was stirred for 30 min, then filtered and the violet filtrate was layered with Et_2O/*n*-hexane (5 mL/5 mL). Violet crystals of **2**·2MeOH were obtained after three days, they were collected by filtration, washed with Et_2O (2 × 5 mL) and dried *in vacuo*. Yield *ca.* 80% (based on the metal). Anal. calcd for **2** (found values in parentheses): C 53.13 (53.48), H 3.96 (3.82), N 13.77 (13.99)%. IR bands (KBr, cm^{-1}): 3342mb, 3148m, 2980w, 2923w, 1616w, 1590w, 1488m, 1452w, 1424w, 1276w, 1168m, 1126s, 1072s, 1038s, 932m, 828m, 760s, 692m, 646m, 512m, 375w.

Synthesis of $[Cu(BF_4)_2(HL)_4]{\cdot}2EtOH$ (3·2EtOH). Solid $Cu(BF_4)_2{\cdot}6H_2O$ (0.138 g, 0.40 mmol) was added under stirring to a solution of HL (0.144 g, 1.00 mmol) in EtOH (25 mL). The resultant green solution was stirred for 30 min, then filtered and stored in a closed vial at room temperature. Light violet crystals of **3**·2EtOH were obtained after six days, they were collected by filtration, washed with Et_2O (2 × 5 mL) and dried *in vacuo*. Yield *ca.* 65% (based on HL). Anal. calcd for **3** (found values in parentheses): C 53.13 (53.41), H 3.96 (3.86), N 13.77 (13.94)%. Selected IR bands (KBr, cm^{-1}): 3346mb, 3148m, 1614w, 1592w, 1490m, 1454m, 1276w, 1168m, 1130s, 1074s, 1040s, 932m, 760s, 692m, 646m, 520m.

Synthesis of $[Cu(BF_4)_2(HL)_4]{\cdot}2$(1-PrOH) [4·2(1-PrOH)]. Solid $Cu(BF_4)_2{\cdot}6H_2O$ (0.138 g, 0.40 mmol) was added under stirring to a solution of HL (0.144 g, 1.00 mmol) in 1-PrOH (25 mL). The resultant blue-green solution was stirred for 30 min, then filtered and stored in a closed vial at room temperature. Light violet crystals of **4**·2(1-PrOH) were obtained after three days, they were collected by filtration, washed with Et_2O (2 × 5 mL) and dried *in vacuo*. Yield *ca.* 65% (based on HL). Anal. calcd for **4**·2(1-PrOH) (found values in parentheses): C 54.01 (53.81), H 5.18 (5.08), N 12.00 (12.31)%. Selected IR bands (KBr, cm^{-1}): 3342mb, 3148 m, 1616w, 1590w, 1488 m, 1452 m, 1276w, 1168 m, 1126s, 1072s, 1040s, 932 m, 760 s, 692 m, 646 m, 512w.

Synthesis of $[Cu(BF_4)_2(HL)_4]{\cdot}1.4$(2-PrOH) [5·1.4(2-PrOH)]. Solid $Cu(BF_4)_2{\cdot}6H_2O$ (0.138 g, 0.40 mmol) was added under stirring to a solution of HL (0.144 g, 1.00 mmol) in 2-PrOH (25 mL). The resultant blue solution was stirred for 30 min, then filtered and the violet filtrate was layered with *n*-hexane (5 mL/5 mL). Violet crystals of **5**·1.4(2-PrOH) were obtained after six days, they were collected by filtration, washed with Et_2O (2 × 5 mL) and dried *in vacuo*. Yield *ca.* 45% (based on HL). Anal. calcd for **5** (found values in parentheses): C 53.13 (52.86), H 3.96 (3.84), N 13.77 (14.07)%. Selected IR bands (KBr, cm^{-1}): 3440mb, 3146mb, 1486m, 1450m, 1173m, 1125s, 1069s, 1038s, 930m, 761s, 684m, 642m, 515m.

Synthesis of $[Cu(BF_4)_2(HL)_4]{\cdot}2$(1-BuOH) [6·2(1-BuOH)]. Solid $Cu(BF_4)_2{\cdot}6H_2O$ (0.086 g, 0.25 mmol) was added under stirring to a solution of HL (0.144 g, 1.00 mmol) in 1-BuOH (25 mL). The resultant violet slurry was stirred for 30 min, then filtered and the clear blue filtrate was layered with *n*-hexane (5 mL/5 mL). Light violet crystals of **6**·2(1-BuOH)

 This journal is © The Royal Society of Chemistry 2024

Open Access Article. Published on 07 June 2024. Downloaded on 7/31/2025 6:43:31 AM. This article is licensed under a Creative Commons Attribution 3.0 Unported Licence.

were obtained after three days, they were collected by filtration, washed with Et_2O (2 × 5 mL) and dried *in vacuo*. Yield *ca.* 45% (based on the metal). Anal. calcd for **6**·2(1-BuOH) (found values in parentheses): C 54.93 (54.61), H 3.96 (3.81), N 11.65 (11.97)%. Selected IR bands (KBr, cm^{-1}): 3425mb, 3140mb, 1490 m, 1448m, 1169m, 1128s, 1071s, 1041s, 927m, 759s, 680m, 645m, 517m.

Synthesis of $[Cu(BF_4)_2(HL)_4]$·2(iso-BuOH) [7·2(iso-BuOH)]. Solid $Cu(BF_4)_2·6H_2O$ (0.086 g, 0.25 mmol) was added under stirring to a solution of HL (0.144 g, 1.00 mmol) in iso-BuOH (25 mL). The resultant mauve slurry was stirred for 30 min, then filtered and the clear pale blue filtrate was layered with *n*-hexane (5 mL/5 mL). Pale purple crystals of **7**·2(iso-BuOH) were obtained after three days, they were collected by filtration, washed with Et_2O (2 × 5 mL) and dried *in vacuo*. Yield *ca.* 50% (based on the metal). Anal. calcd for **7**·2(iso-BuOH) (found values in parentheses): C 54.93 (54.61), H 5.45 (5.62), N 11.65 (11.97)%. Selected IR bands (KBr, cm^{-1}): 3338mb, 3126m, 1492m, 1456m, 1178m, 1126s, 1070s, 1041s, 932m, 772s, 698m, 646m, 518w.

Synthesis of $[Cu(BF_4)_2(HL)_4]$·1.33(*tert*-BuOH) [8·1.33(*tert*-BuOH)]. Solid $Cu(BF_4)_2·6H_2O$ (0.086 g, 0.25 mmol) was added under stirring to a solution of HL (0.144 g, 1.00 mmol) in *tert*-BuOH (25 mL). The resultant dark violet solution was stirred for 30 min, then filtered and stored in a closed vial at room temperature. Violet crystals of **8**·1.33(*tert*-BuOH) were obtained after three days, they were collected by filtration, washed with Et_2O (2 × 5 mL) and dried *in vacuo*. Yield *ca.* 35% (based on the metal). Anal. calcd for **8** (found values in parentheses): C 53.13 (53.49), H 3.96 (3.75), N 13.77 (13.43)%. Selected IR bands (KBr, cm^{-1}): 3430sb, 3138mb, 1488m, 1446m, 1173m, 1131s, 1074s, 1045s, 931m, 757m, 684m, 644m, 520w.

Synthesis of $[Cu(BF_4)_2(HL)_4]$·2(1-PeOH) [9·2(1-PeOH)]. Solid $Cu(BF_4)_2·6H_2O$ (0.138 g, 0.40 mmol) was added under stirring to a solution of HL (0.144 g, 1.00 mmol) in 1-PeOH (25 mL). The resultant lilac slurry was stirred for 30 min, then filtered and the pale green filtrate was layered with Et_2O (5 mL/5 mL). Mauve crystals of **9**·2(1-PeOH) were obtained after five months, they were collected by filtration, washed with Et_2O (2 × 5 mL) and dried *in vacuo*. Yield *ca.* 40% (based on the ligand). Anal. calcd for **9**·2(1-PeOH) (found values in parentheses): C 55.80 (55.44), H 5.70 (5.60), N 11.32 (11.61)%. Selected IR bands (KBr, cm^{-1}): 3418sb, 3127mb, 1492m, 1444m, 1170m, 1134s, 1079s, 1043s, 928m, 762s, 682m, 641m, 516w.

Synthesis of $[Cu(BF_4)_2(HL)_4]$·2DMF (10·2DMF). Solid $Cu(BF_4)_2·6H_2O$ (0.086 g, 0.25 mmol) was added under stirring to a solution of HL (0.144 g, 1.00 mmol) in CH_2Cl_2/DMF (25 mL/3 mL). The mixture was stirred for 40 min, the resultant blue solution was filtered and the violet filtrate was layered with Et_2O/*n*-hexane (5 mL/5 mL). Violet crystals of **10**·2DMF were obtained after three days, they were collected by filtration, washed with Et_2O (2 × 5 mL) and dried *in vacuo*. Yield *ca.* 70% (based on the metal). Anal. calcd for **10**·2DMF (found values in parentheses): C 52.55 (52.31), H 4.83 (4.70), N 14.59 (14.89)%. Selected IR bands (KBr, cm^{-1}): 3148m, 1650s, 1614m, 1590m, 1492m, 1454m, 1388m, 1170 m, 1130s, 1072s, 1038s, 964m, 762s, 692m, 648 m, 520w.

Synthesis of $[Cu(BF_4)_2(HL)_4]$·1.2Me_2CO (11·1.2Me_2CO). Solid $Cu(BF_4)_2·6H_2O$ (0.138 g, 0.40 mmol) was added under stirring to a solution of HL (0.144 g, 1.0 mmol) in Me_2CO (25 mL). The resultant green solution was stirred for 30 min, then filtered and the violet filtrate was layered with *n*-hexane (5 mL/5 mL). Light violet crystals of **11**·1.2Me_2CO were obtained after eight days, they were collected by filtration, washed with Et_2O (2 × 5 mL) and dried *in vacuo*. Yield *ca.* 60% (based on HL). Anal. calcd for **11** (found values in parentheses): C 53.13 (52.82), H 3.96 (3.80), N 13.77 (14.09)%. Selected IR bands (KBr, cm^{-1}): 3130mb, 1674s, 1491m, 1440m, 1168m, 1137s, 1074s, 1041s, 932m, 761s, 679m, 642m, 518m.

Synthesis of $[Cu(BF_4)_2(HL)_4]$·2THF (12·2THF). Solid $Cu(BF_4)_2·6H_2O$ (0.086 g, 0.25 mmol) was added under stirring to a solution of HL (0.144 g, 1.00 mmol) in THF (25 mL). The resultant dark violet solution was stirred for 30 min and a violet slurry appeared, which was then filtered and the clear violet filtrate was layered with Et_2O (5 mL/5 mL). Violet crystals of **12**·2THF were obtained after five days, they were collected by filtration, washed with Et_2O (2 × 5 mL) and dried *in vacuo*. Yield *ca.* 65% (based on the metal). Anal. calcd for **12** (found values in parentheses): C 53.13 (53.46), H 3.96 (3.87), N 13.77 (12.81)%. Selected IR bands (KBr, cm^{-1}): 3122mb, 1489m, 1441m, 1169m, 1141s, 1078s, 1044s, 930m, 759s, 680m, 640m, 512w.

Synthesis of $[Cu(BF_4)_2(HL)_4]$·1.85(1,4-dioxane) [13·1.85(1,4-dioxane)]. Solid $Cu(BF_4)_2·6H_2O$ (0.086 g, 0.25 mmol) was added under stirring to a solution of HL (0.144 g, 1.00 mmol) in 1,4-dioxane (25 mL). The resultant violet solution was stirred for 30 min and a violet slurry appeared, which was then filtered and the clear light violet filtrate was layered with Et_2O (5 mL/5 mL). Violet/pink crystals of **13**·1.85(1,4-dioxane) were obtained after four days, they were collected by filtration, washed with Et_2O (2 × 5 mL) and dried *in vacuo*. Yield *ca.* 60% (based on the metal). Anal. calcd for **13**·1.85(1,4-dioxane) (found values in parentheses): C 53.35 (52.97), H 4.84 (5.02), N 11.47 (11.19)%. Selected IR bands (KBr, cm^{-1}): 3134mb, 1484m, 1450m, 1167m, 1129s, 1071s, 1043s, 927m, 756m, 678m, 642m, 523m.

Synthesis of $[Cu(BF_4)_2(HL)_4]$·0.86EtOAc (14·0.86EtOAc). Solid $Cu(BF_4)_2·6H_2O$ (0.086 g, 0.25 mmol) was added under stirring to a solution of HL (0.144 g, 1.00 mmol) in ethyl acetate (25 mL). The resultant mauve slurry was stirred for 30 min and a violet solid appeared which was then filtered; the pale violet filtrate was stored at low temperature (5 °C). Violet crystals of **14**·0.86EtOAc were obtained after five days, they were collected by filtration, washed with Et_2O (2 × 5 mL) and dried *in vacuo*. Yield *ca.* 45% (based on the metal). Anal. calcd for **14** (found values in parentheses): C 53.13 (52.79), H 3.96 (3.82), N 13.77 (14.09)%. Selected IR bands (KBr, cm^{-1}): 3128mb, 1701m, 1482m, 1449m, 1171m, 1126s, 1073s, 1045s, 931m, 755m, 679m, 648m, 514w.

Open Access Article. Published on 07 June 2024. Downloaded on 7/31/2025 6:43:31 AM. This article is licensed under a Creative Commons Attribution 3.0 Unported Licence.

Synthesis of $[Cu(BF_4)_2(HL)_4]\cdot Et_2O$ (15·Et_2O). Solid $Cu(BF_4)_2\cdot 6H_2O$ (0.086 g, 0.25 mmol) was added under stirring to a solution of HL (0.144 g, 1.00 mmol) in iso-pentanol (25 mL). The resultant blue/green solution was stirred for 30 min, then filtered and the violet filtrate was layered with Et_2O (5 mL/5 mL). Violet crystals of **15**·Et_2O were obtained after five days, they were collected by filtration, washed with Et_2O (2 × 5 mL) and dried *in vacuo*. Yield *ca.* 70% (based on the metal). Anal. calcd for **15** (found values in parentheses): C 53.13 (53.39), H 3.96 (3.80), N 13.77 (14.12)%. Selected IR bands (KBr, cm^{-1}): 3135mb, 1479m, 1450m, 1169m, 1130s, 1071s, 1042s, 930m, 757s, 676m, 644m, 515w.

Synthesis of $[Cu(BF_4)_2(HL)_4]\cdot 0.7$DIPE (16·0.7DIPE). Solid $Cu(BF_4)_2\cdot 6H_2O$ (0.086 g, 0.25 mmol) was added under stirring to a solution of HL (0.144 g, 1.00 mmol) in nitromethane (25 mL). The resultant pale blue solution was stirred for 75 min and a dark blue/green slurry appeared which was then filtered; the clear dark blue/green filtrate was layered with diisopropyl ether (DIPE) (5 mL/5 mL). Violet crystals of **16**·0.7DIPE were obtained after seven days, they were collected by filtration, washed with Et_2O (2 × 5 mL) and dried *in vacuo*. Yield *ca.* 40% (based on the metal). Anal. calcd for **16** (found values in parentheses): C 53.13 (53.43), H 3.96 (3.81), N 13.77 (14.10)%. Selected IR bands (KBr, cm^{-1}): 3152mb, 1482m, 1451m, 1171m, 1128s, 1069s, 1046s, 928m, 756s, 674m, 645m, 515w.

Synthesis of $[Cu(BF_4)_2(HL)_4]\cdot$(*n*-hexane) [17·(*n*-hexane)]. Solid $Cu(BF_4)_2\cdot 6H_2O$ (0.086 g, 0.25 mmol) was added under stirring to a solution of HL (0.144 g, 1.00 mmol) in *tert*-BuOH (25 mL). The resultant dark blue solution was stirred for 30 min, then filtered and the violet filtrate was layered with *n*-hexane (5 mL/5 mL). Violet crystals of **17**·(*n*-hexane) were obtained after five days, they were collected by filtration, washed with Et_2O (2 × 5 mL) and dried *in vacuo*. Yield *ca.* 40% (based on the metal). Anal. calcd for **17** (found values in parentheses): C 53.13 (53.50), H 3.96 (3.79), N 13.77 (13.50)%. Selected IR bands (KBr, cm^{-1}): 3149mb, 2940m, 1480m, 1449m, 1169m, 1127s, 1074s, 1044s, 930m, 757s, 672m, 643m, 516w.

Synthesis of $[Cu(HL)_4(MeCN)(H_2O)_{0.4}](BF_4)_2$ (18). Solid $Cu(BF_4)_2\cdot 6H_2O$ (0.086 g, 0.25 mmol) was added under stirring to a solution of HL (0.144 g, 1.00 mmol) in CH_2Cl_2/MeCN (20 mL/5 mL). The resultant dark mauve slurry was stirred for 30 min, then filtered and the clear mauve filtrate was layered with Et_2O/*n*-hexane (5 mL/5 mL). Violet crystals of **18** were obtained after four days, they were collected by filtration, washed with Et_2O (2 × 5 mL) and dried *in vacuo*. Yield *ca.* 60% (based on the metal). Anal. calcd for **18** (found values in parentheses): C 52.89 (52.61), H 4.19 (3.99), N 14.62 (14.96)%. Selected IR bands (KBr, cm^{-1}): 3435wb, 3150wb, 2170w, 1479m, 1451m, 1167m, 1130s, 1076s, 1042s, 928m, 759s, 670m, 647m, 518w.

Synthesis of $[Cu\{SiF_2O(OMe)\}_2(HL)_4]\cdot 0.8MeNO_2$ (19·0.8$MeNO_2$). Solid $Cu(BF_4)_2\cdot 6H_2O$ (0.086 g, 0.25 mmol) was added under stirring to a solution of HL (0.144 g, 1.00 mmol) in $MeNO_2$ (25 mL). The resultant dark blue/green slurry was stirred for 75 min, then filtered and the clear blue/green filtrate was stored at low temperature (5 °C). Violet crystals of **19**·0.8$MeNO_2$ were obtained after a week, they were collected by filtration, washed with Et_2O (2 × 5 mL) and dried *in vacuo*. Yield *ca.* 60% (based on the metal). Anal. calcd for **19**·0.8$MeNO_2$ (found values in parentheses): C 50.87 (51.22), H 4.41 (4.19), N 13.46 (13.11)%. Selected IR bands (KBr, cm^{-1}): 3150mb, 1561m, 1479m, 1482m, 1440m, 1376m, 1168m, 1128s, 1072s, 1043m, 1026m, 931m, 758m, 669m, 648m, 517w.

X-ray crystallography

Suitable single-crystals of the compounds, covered with paratone-N oil, were mounted in cryo-loops at the end of a copper pin. Diffraction data were collected (ω-scans technique) on a SuperNova Rigaku diffractometer under a flow of nitrogen gas at 100(2) K using Mo Kα radiation (λ = 0.7107 Å), with the exception of compounds **5**·1.4(2-PrOH) and **9**·2(1-PeOH), for which Cu Kα radiation (λ = 1.5418 Å) was used. Crystallographic data are listed in Table 1. Data were collected and processed by the CRYSALIS CCD and RED software,[53] respectively; the reflection intensities were corrected for absorption by the multiscan method. The structures were solved using direct methods (SIR92 (ref. 54) and SHELXT[55]) or the charge flipping algorithm (Superflip[56,57]) and the models were refined by full-matrix least-squares on F^2 with SHELXL-2019/3.[58] All non-H atoms were refined anisotropically; carbon-bound H-atoms were introduced at calculated positions and allowed to ride on their carrier atoms (riding model). The structure of **16** was refined as a non-merohedral twin with a 32 : 68 components ratio. All imidazole H-atoms on the pyrrolic-type N1 atom of the ligands, together with the hydroxyl H-atoms of the protic solvents in compounds **2**–**9** and the water H-atoms in compounds **1** and **18** were located in difference Fourier maps, and refined isotropically applying soft distance restraints (DFIX). Considerable disorder has been observed in most of the crystal structures. A two-part disorder model was applied to the BF_4^- ions in complexes **1**, **2**, **3**, **7**, **10**, **11** and **13**, while the highly disordered BF_4^- ion in complex **5** is best modelled over three sites (three-component model). Similar treatment has been applied for the analogous disordered $\{SiF_2O(OMe)\}^-$ ion in compound **19**. The HL ligands are also affected by positional disorder: this includes the phenyl ring in molecules **5** (triply disordered), **7**, **13** and **15** (two sites) and the entire HL ligand in complex **11**. Partial occupancies have been assigned after detailed refinement for the solvent molecules in compounds **5**·1.4(2-PrOH), **11**·1.2Me_2CO, **13**·1.85(1,4-dioxane), **14**·0.86EtOAc, **16**·0.7DIPE and **19**·0.8$MeNO_2$. The solvents in **3**·2EtOH, **7**·2(iso-BuOH), **9**·2(1-PeOH), **12**·2THF, **14**·0.86EtOAc, **15**·Et_2O, **16**·0.7DIPE and the coordinated MeCN in complex **18** have also been modelled over two sites; of these, the EtOAc, Et_2O and DIPE solvents (in complexes **14**, **15** and **16**, respectively) are orientationally disordered about an inversion centre and the coordinated MeCN (in complex **18**) about a two-fold axis.

Geometric/crystallographic calculations were carried out using PLATON,[59] OLEX2 (ref. 60) and WINGX[61] packages;

 This journal is © The Royal Society of Chemistry 2024

Open Access Article. Published on 07 June 2024. Downloaded on 7/31/2025 6:43:31 AM.
This article is licensed under a Creative Commons Attribution 3.0 Unported Licence.

Table 1 Crystallographic data for compounds **1**·2Me_2CO·2H_2O–**19**·0.8$MeNO_2$

Compound reference	**1**·2Me_2CO·2H_2O	**2**·2MeOH	**3**·2EtOH	**4**·2(1-PrOH)	**5**·1.4(2-PrOH)
Chemical formula	$C_{36}H_{32}B_2CuF_8N_8$·2(C_3H_6O)·2(H_2O)	$C_{36}H_{32}B_2CuF_8N_8$·2(CH_4O)	$C_{36}H_{32}B_2CuF_8N_8$·2(C_2H_6O)	$C_{36}H_{32}B_2CuF_8N_8$·2(C_3H_8O)	$C_{36}H_{32}B_2CuF_8N_8$·1.4(C_3H_8O)
Formula mass/g mol^{-1}	966.04	877.94	905.99	934.04	897.99
Crystal system	Monoclinic	Triclinic	Triclinic	Triclinic	Triclinic
Space group	$P2_1/c$	$P\bar{1}$	$P\bar{1}$	$P\bar{1}$	$P\bar{1}$
a/Å	8.8391(5)	8.8582(4)	8.9408(8)	9.1101(3)	9.0160(8)
b/Å	26.4003(12)	9.5536(7)	9.5997(11)	9.9335(4)	9.6842(7)
c/Å	9.9765(5)	13.4305(9)	13.2336(9)	13.3316(6)	13.7262(8)
α/°	90	105.470(6)	104.392(8)	104.812(4)	69.875(6)
β/°	106.136(5)	92.908(5)	92.473(7)	94.552(3)	80.108(7)
γ/°	90	107.642(5)	106.907(9)	104.842(4)	72.626(7)
Unit cell volume/$Å^3$	2236.3(2)	1033.13(12)	1044.43(18)	1113.81(8)	1070.77(15)
Z, Z'	2, 0.5	1, 0.5	1, 0.5	1, 0.5	1, 0.5
Temperature/K	100(2)	100(2)	100(2)	100(2)	100(2)
Radiation type, μ/mm^{-1}	MoKα, 0.573	MoKα, 0.609	MoKα, 0.605	MoKα, 0.569	CuKα, 1.400
No. of reflections measured	14 738	7482	7679	9553	6493
No. of independent reflections	4369	4053	3665	4810	3806
R_{int}	0.073	0.027	0.038	0.036	0.046
Final R_1 values ($I > 2\sigma(I)$)	0.0442	0.0442	0.0667	0.0431	0.0845
Final w$R(F^2)$ values ($I > 2\sigma(I)$)	0.0839	0.0983	0.1458	0.0970	0.2183
Final R_1 values (all data)	0.0715	0.0509	0.0867	0.0557	0.0962
Final w$R(F^2)$ values (all data)	0.0925	0.1036	0.1626	0.1051	0.2317
Goodness of fit on F^2	1.025	1.056	1.055	1.072	1.026
$\Delta\rho_{max}$, $\Delta\rho_{min}$/e $Å^{-3}$	0.369, −0.500	0.446, −0.518	0.812, −0.724	0.577, −0.504	0.781, −0.646
CCDC number	2342307	2342308	2 342 309	2 342 310	2 342 311

Compound reference	**6**·2(1-BuOH)	**7**·2(iso-BuOH)	**8**·1.33(*tert*-BuOH)	**9**·2(1-PeOH)	**10**·2DMF
Chemical formula	$C_{36}H_{32}B_2CuF_8N_8$·2($C_4H_{10}O$)	$C_{36}H_{32}B_2CuF_8N_8$·2($C_4H_{10}O$)	$C_{36}H_{32}B_2CuF_8N_8$·1.33($C_4H_{10}O$)	$C_{36}H_{32}B_2CuF_8N_8$·2($C_5H_{12}O$)	$C_{36}H_{32}B_2CuF_8N_8$·2(C_3H_7NO)
Formula mass/g mol^{-1}	962.09	962.09	912.68	990.14	960.05
Crystal system	Triclinic	Triclinic	Triclinic	Triclinic	Triclinic
Space group	$P\bar{1}$	$P\bar{1}$	$P\bar{1}$	$P\bar{1}$	$P\bar{1}$
a/Å	9.2340(6)	9.2904(12)	15.0482(5)	9.3029(7)	9.0724(7)
b/Å	9.9950(8)	9.9448(16)	15.3209(5)	9.9439(8)	9.8173(7)
c/Å	13.3246(9)	14.0725(19)	16.1054(7)	14.3527(11)	14.3397(9)
α/°	105.451(6)	110.200(13)	103.710(3)	73.234(7)	75.963(6)
β/°	94.995(5)	94.866(11)	110.373(4)	73.473(7)	71.693(6)
γ/°	104.322(6)	105.768(12)	100.587(3)	73.130(7)	71.238(7)
Unit cell volume/$Å^3$	1132.98(15)	1151.1(3)	3234.0(2)	1187.02(17)	1133.80(15)
Z, Z'	1, 0.5	1, 0.5	3, 1.5	1, 0.5	1, 0.5
Temperature/K	100(2)	100(2)	100(2)	100(2)	100(2)
Radiation type, μ/mm^{-1}	MoKα, 0.562	MoKα, 0.553	MoKα, 0.585	CuKα, 1.323	MoKα, 0.563
No. of reflections measured	8034	8798	29 587	7751	9021
No. of independent reflections	3926	4261	12 042	4456	4665
R_{int}	0.070	0.061	0.057	0.022	0.028
Final R_1 values ($I > 2\sigma(I)$)	0.0634	0.0565	0.0573	0.0347	0.0401
Final $wR(F^2)$ values ($I > 2\sigma(I)$)	0.1504	0.1292	0.1353	0.0872	0.0911
Final R_1 values (all data)	0.0861	0.0796	0.0867	0.0401	0.0496
Final $wR(F^2)$ values (all data)	0.1593	0.1503	0.1558	0.0922	0.1003
Goodness of fit on F^2	1.182	1.051	1.038	1.054	1.015

Open Access Article. Published on 07 June 2024. Downloaded on 7/31/2025 6:43:31 AM.
This article is licensed under a Creative Commons Attribution 3.0 Unported Licence.

Table 1 *(continued)*

Compound reference	**6**·2(1-BuOH)	**7**·2(iso-BuOH)	**8**·1.33(*tert*-BuOH)	**9**·2(1-PeOH)	**10**·2DMF
$\Delta\rho_{max}$, $\Delta\rho_{min}$/e Å^{-3}	0.491, −0.543	0.394, −1.008	1.081, −0.614	0.341, −0.373	0.482, −0.447
CCDC number	2342312	2342313	2342314	2342315	2342316

Compound reference	**11**·1.2Me$_2$CO	**12**·2THF	**13**·1.85(1,4-dioxane)	**14**·0.86EtOAc	**15**·Et$_2$O
Chemical formula	$C_{36}H_{32}B_2CuF_8N_8$·1.2(C_3H_6O)	$C_{36}H_{32}B_2CuF_8N_8$·2(C_4H_8O)	$C_{36}H_{32}B_2CuF_8N_8$·1.85($C_4H_8O_2$)	$C_{36}H_{32}B_2CuF_8N_8$·0.86($C_4H_8O_2$)	$C_{36}H_{32}B_2CuF_8N_8$·$C_4H_{10}O$
Formula mass/g mol^{-1}	883.55	958.06	976.85	889.62	887.97
Crystal system	Triclinic	Triclinic	Triclinic	Triclinic	Triclinic
Space group	$P\bar{1}$	$P\bar{1}$	$P\bar{1}$	$P\bar{1}$	$P\bar{1}$
a/Å	8.950(3)	9.4113(9)	9.2398(7)	8.6393(5)	8.5831(9)
b/Å	9.655(3)	10.2218(12)	9.9904(9)	9.7696(6)	9.7612(11)
c/Å	13.284(4)	12.8120(12)	12.6976(12)	12.8911(8)	12.8928(11)
α/°	73.31(3)	87.054(9)	78.043(8)	99.164(5)	98.221(8)
β/°	87.75(2)	75.179(9)	85.634(7)	93.555(5)	93.854(8)
γ/°	72.57(3)	70.705(10)	73.908(7)	106.361(6)	107.301(10)
Unit cell volume/Å^3	1047.6(5)	1123.8(2)	1101.53(17)	1024.08(11)	1013.80(19)
Z, Z'	1, 0.5	1, 0.5	1, 0.5	1, 0.5	1, 0.5
Temperature/K	100(2)	100(2)	100(2)	100(2)	100(2)
Radiation type, μ/mm^{-1}	MoKα, 0.600	MoKα, 0.566	MoKα, 0.582	MoKα, 0.615	MoKα, 0.620
No. of reflections measured	7907	9610	8689	6976	7573
No. of independent reflections	3654	4635	3848	3594	4186
R_{int}	0.075	0.046	0.052	0.028	0.038
Final R_1 values ($I > 2\sigma(I)$)	0.0891	0.0565	0.0898	0.0555	0.0466
Final w$R(F^2)$ values ($I > 2\sigma(I)$)	0.2167	0.1380	0.2293	0.1438	0.0922
Final R_1 values (all data)	0.1478	0.0761	0.1355	0.0619	0.0703
Final w$R(F^2)$ values (all data)	0.2647	0.1537	0.2690	0.1500	0.1025
Goodness of fit on F^2	1.043	1.061	1.020	1.045	1.033
$\Delta\rho_{max}$, $\Delta\rho_{min}$/e Å^{-3}	0.773, −0.742	0.538, −0.541	0.895, −0.703	1.144, −1.149	0.524, −0.426
CCDC number	2342317	2342318	2342319	2342320	2342321

Compound reference	**16**·0.7DIPE	**17**·(*n*-hexane)	**18**	**19**·0.8MeNO$_2$
Chemical formula	$C_{36}H_{32}B_2CuF_8N_8$·0.70($C_6H_{14}O$)	$C_{36}H_{32}B_2CuF_8N_8$·C_6H_{14}	$C_{38}H_{35.80}CuN_9O_{0.40}(BF_4)_2$	$C_{38}H_{38}CuF_4N_8O_4Si_2$·0.8($CH_3NO_2$)
Formula mass/g mol^{-1}	885.37	900.03	862.11	915.32
Crystal system	Triclinic	Triclinic	Orthorhombic	Monoclinic
Space group	$P\bar{1}$	$P\bar{1}$	*Pnn*2	*P*2/*n*
a/Å	8.7016(6)	8.7411(10)	11.1724(4)	17.5681(7)
b/Å	9.8158(8)	9.7698(14)	12.3470(6)	9.8878(3)
c/Å	12.9608(14)	12.811(2)	13.8235(6)	24.2057(9)
α/°	96.464(8)	97.513(13)	90	90
β/°	96.268(8)	93.679(12)	90	96.253(3)
γ/°	106.150(7)	107.576(12)	90	90
Unit cell volume/Å^3	1045.07(16)	1027.8(3)	1906.89(14)	4179.8(3)
Z, Z'	1, 0.5	1, 0.5	2, 0.5	4, 1
Temperature/K	100(2)	100(2)	100(2)	100(2)
Radiation type, μ/mm^{-1}	MoKα, 0.600	MoKα, 0.610	MoKα, 0.656	MoKα, 0.654
No. of reflections measured	3674	7520	10 413	37 126
No. of independent reflections	3674	4022	4140	37 126
R_{int}	—	0.032	0.042	0.054
Final R_1 values ($I > 2\sigma(I)$)	0.0855	0.0508	0.0453	0.0610
Final w$R(F^2)$ values ($I > 2\sigma(I)$)	0.2155	0.1155	0.1162	0.1546

This journal is © The Royal Society of Chemistry 2024

Open Access Article. Published on 07 June 2024. Downloaded on 7/31/2025 6:43:31 AM.
This article is licensed under a Creative Commons Attribution 3.0 Unported Licence.

Table 1 *(continued)*

Compound reference	**16**·0.7DIPE	**17**·(*n*-hexane)	**18**	**19**·0.8$MeNO_2$
Final R_1 values (all data)	0.1009	0.0640	0.0543	0.0778
Final w$R(F^2)$ values (all data)	0.2269	0.1261	0.1259	0.1676
Goodness of fit on F^2	1.101	1.060	1.021	1.061
$\Delta\rho_{max}$, $\Delta\rho_{min}$/e Å^{-3}	1.339, −1.089	1.473, −0.997	0.636, −0.410	1.057, −0.693
CCDC number	2342322	2342323	2342324	2342325

molecular/packing graphics were prepared with MERCURY.[62] Photos of the crystals are shown in Fig. S1.†

Results and discussion

Synthetic comments

A variety of reactions were initially studied with the aim of preparing the largest possible number of complexes exploring the Cu(II)/HL/tetrafluoroborate system. Our trials included differing reactant ratios and concentrations, solvents, crystallization conditions and temperatures. It soon turned out that the reaction system yielded solvatomorphic compounds of the general formula $[Cu(BF_4)_2(HL)_4]\cdot x$(solvent). Utilizing a variety of crystallization solvents (polar protic, polar aprotic and non-polar) a series of seventeen crystalline solvatomorphs have been isolated. The general synthetic route with the individual formulae of the resulting complexes are illustrated in Scheme 1. A schematic illustration of the molecular structure of the solvatomorphs is shown in Scheme 2. Cu(II) is air stable and the synthetic work was thus conducted under aerobic conditions in the normal laboratory atmosphere. Attempts with iso-pentanol (**15**), $MeNO_2$ (**16**) and *tert*-BuOH (**17**) as main reaction solvents did not produce exactly the anticipated solvatomorphs with respect to the included solvents; instead, the solvents used in the layering technique for crystal growth were found within the crystals, resulting in the **15**·Et_2O, **16**·0.7DIPE and **17**·(*n*-hexane) solvatomorphs, respectively. In the synthesis of compound **18**, using CH_2Cl_2/MeCN as reaction solvents, the two tetrafluoroborato ligands in the anticipated $[Cu(BF_4)_2(HL)_4]$ molecule have been replaced by a MeCN and a partially occupied water molecule (40%), producing crystals of the cationic $[Cu(HL)_4(MeCN)(H_2O)_{0.4}](BF_4)_2$ complex (Fig. S2a†). The compounds were obtained by reactions with a metal-to-ligand ratio of 1 : 2.5 or 1 : 4 and have an octahedral geometry at the metal centre; their colour is violet or mauve.

As in all reactions, $Cu(BF_4)_2\cdot 6H_2O$ was used as the metal source in the synthesis of **19**·0.8$MeNO_2$; however, the final crystalline product was identified as $[Cu\{SiF_2O(OMe)\}_2(HL)_4]\cdot 0.8MeNO_2$ (Schemes 3 and 4, Fig. S3a†). The coordinated $\{SiF_2O(OMe)\}^-$ ions, which appear for the first time in coordination chemistry, were

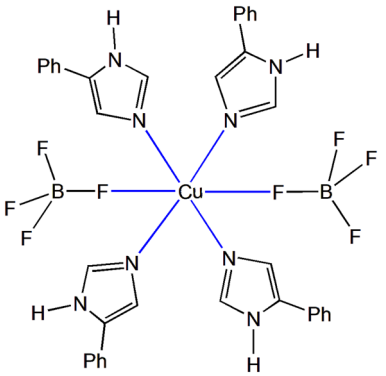

Scheme 2 Schematic representation of the general molecular structure of **1**–**17** which have the same coordination entity.

Open Access Article. Published on 07 June 2024. Downloaded on 7/31/2025 6:43:31 AM.
This article is licensed under a Creative Commons Attribution 3.0 Unported Licence.

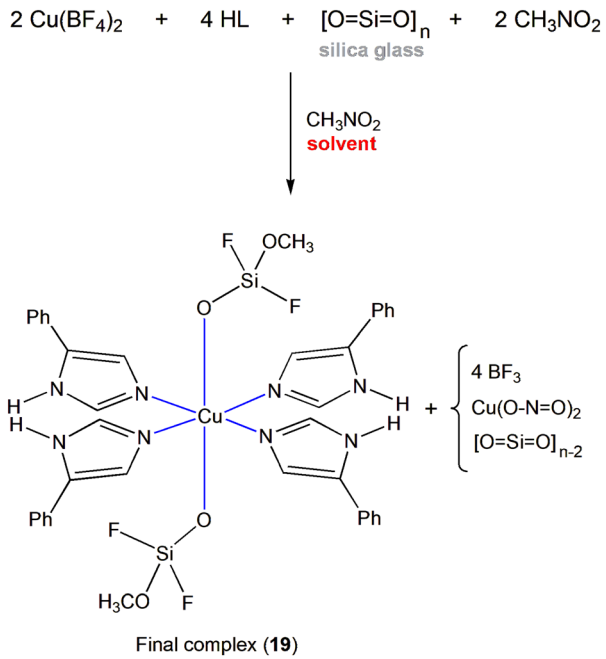

Scheme 3 The overall reaction of $Cu(BF_4)_2$ with 4-phenylimidazole in a glass vessel using nitromethane as solvent. The difluorosilicate dianion is released into the solution upon attack of the glass surface by the 'naked' tetrafluoroborate anion. The final product contains the tautomer 5-phenylimidazole as ligand.

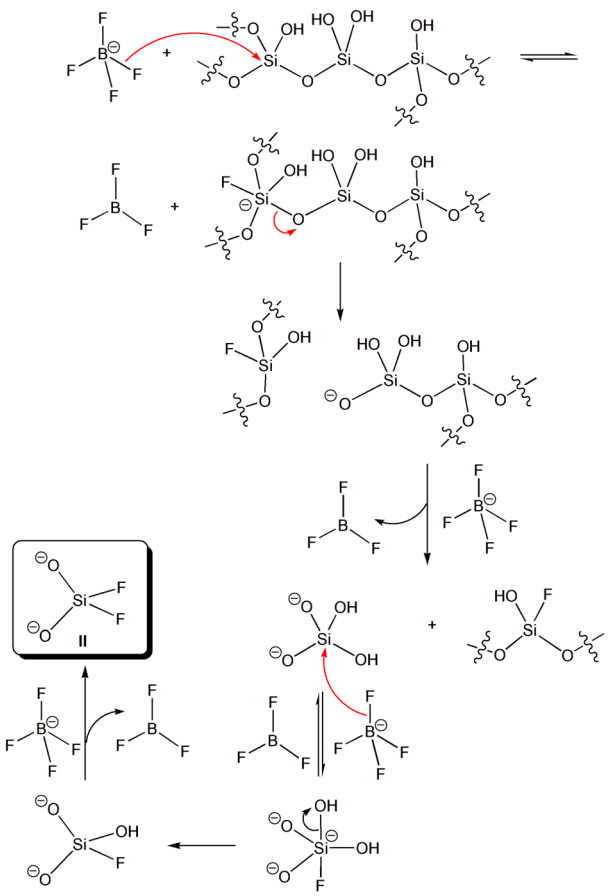

Scheme 4 Simplified mechanism for the liberation of silicate dianions to the nitromethane solution upon attack of tetrafluoroborate anions on the glass surface. The silicate dianions are further attacked by tetrafluoroborate anions to give finally the difluorosilicate dianion **II**.

actually generated *in situ* by the reaction of fluoride anions from BF_4^- with the glass surface of the vial used to grow crystals of the complex. The proposed mechanism (Scheme 5) involves the following steps:

i) Initial formation of the complex **I** in which two molecules of nitromethane act as bidentate ligands and two molecules of 5-phenylimidazole as monodentate ligands. The complexation of nitromethane serves to facilitate the subsequent attack of its methyl group by the difluorosilicate anion.

ii) The difluorosilicate dianion (**II**), released from the glass surface upon attack of silicon atoms on the surface by tetrafluoroborate anions (Scheme 4), then partially displaces the nitromethane from the metal cation leading to the new complex **III**. The driving force for the liberation of the difluorosilicate dianion from the glass surface is the formation of the very strong Si–F bonds.[47]

iii) Facile intramolecular S_N2 reaction of the complexed difluorosilicate anion on the neighbouring methyl group then leads to methylation of the difluorosilicate dianion with simultaneous formation of nitrite anion (complex **IV**). The latter is then displaced by a third molecule of 5-phenylimidazole to provide the new complex **V**.

iv) Steps 2 and 3 are then repeated with a second difluorosilicate dianion to give the final complex through the intermediate complexes **VI** and **VII**.

Four final remarks concerning our above mentioned mechanistic ideas are worthy of note at this point: (a) Further replacement in **II** by fluorides is not probable, because silicon bears a large number of electrons (totally 24!) around it, while O^- is with +I (and +M) effects. Therefore, silicon cannot be attacked by other nucleophiles; moreover, O^{2-} is an extremely bad leaving group, much worse than the already very bad HO^- leaving group. (b) Recent theoretical studies[63] have shown the possibility of gradual replacement of OH groups by F atoms in silicon dioxide until the formation of SiF_4; in the theoretical study, however, the etchant was HF molecule, while in our experimental work the attacking species is F^- (from BF_4^-). The glassware used in our laboratory is borosilicate glass. This has a more complicated structure compared to that of the simple silica glass used in the calculations, because it contains B atoms in the lattice and intermediate Na^+ ions, but again the dominant species is SiO_2. (c) It is well known in organic chemistry that the nitro group can play diverse roles that make several transformations;[64] and (d) Reactions in which fluoride species attack to glassware to form silicon–fluoride compounds have been described in the literature.[48]

All attempts to employ chlorinated compounds (CH_2Cl_2, $CHCl_3$) as crystallization solvents failed to give crystalline materials. Also attempts to prepare solvatomorphs $[Cu(HL)_4(BF_4)_2]$ using DMSO as the reaction solvent were in vain, probably due to the excellent donor capacity of this solvent which is readily coordinated to copper(II) hampering complexation with HL and BF_4^-.

This journal is © The Royal Society of Chemistry 2024

Open Access Article. Published on 07 June 2024. Downloaded on 7/31/2025 6:43:31 AM.
This article is licensed under a Creative Commons Attribution 3.0 Unported Licence.

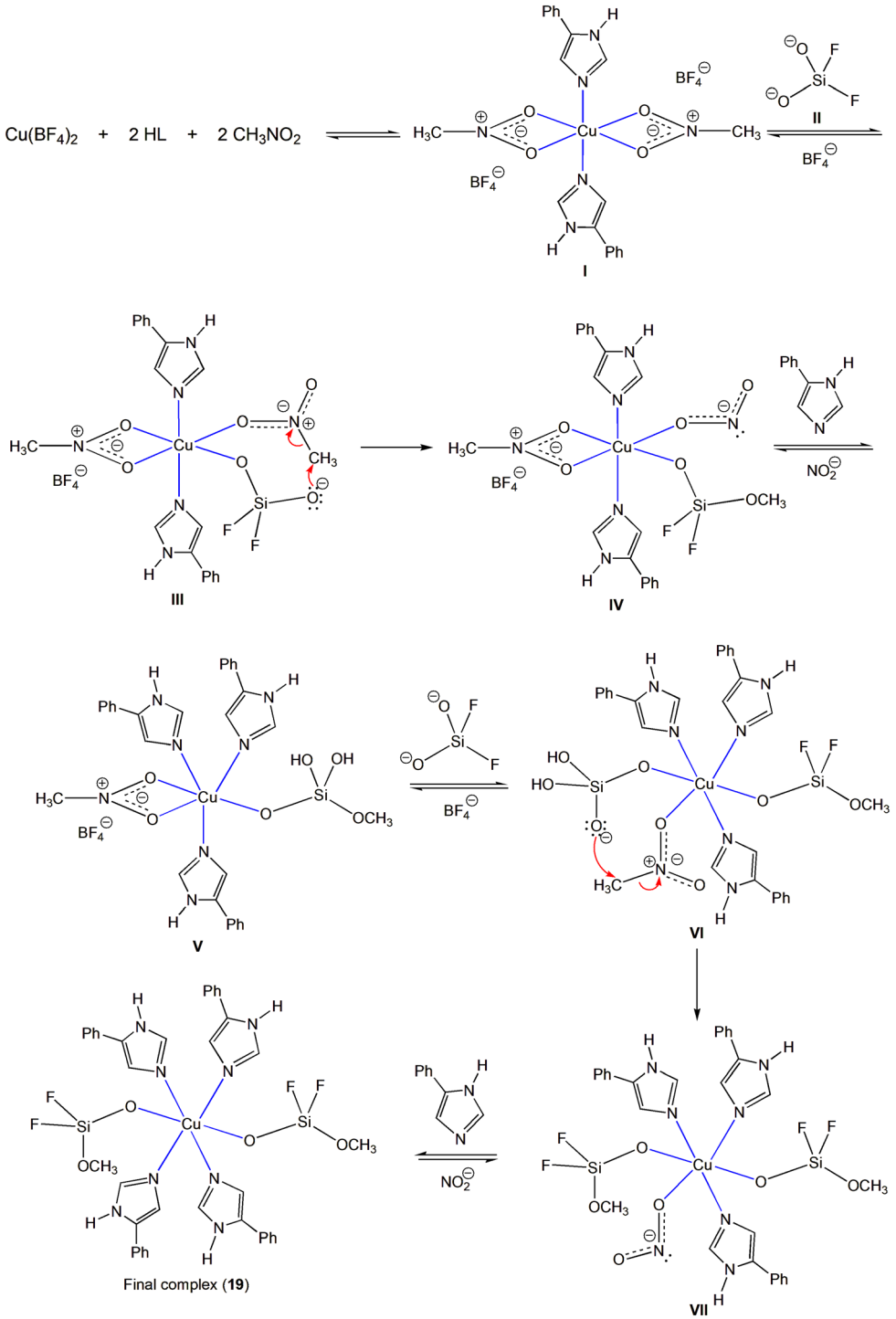

Scheme 5 Proposed mechanism for the formation of the final complex from the reaction of copper(II) tetrafluoroborate with 4-phenylimidazole (HL) in a glass vessel using nitromethane as solvent. We assume that the ligand HL is in its tautomeric 5-phenylimidazole form from the start of the reaction.

All crystalline products were characterized by IR spectroscopy, microanalyses, single-crystal X-ray diffraction and TGA experiments (for selected compounds). Various trials to obtain crystals of the solvent-free forms, including triethyl orthoformate as a drying agent and several solvent mixtures, were in vain.

Description of the structures

To facilitate discussion and molecular comparison, the same numbering scheme has been assigned (where applicable) to the HL ligand atoms and the coordinated tetrafluoroborate ions for all compounds presented herein (Fig. 1).

Open Access Article. Published on 07 June 2024. Downloaded on 7/31/2025 6:43:31 AM.
This article is licensed under a Creative Commons Attribution 3.0 Unported Licence.

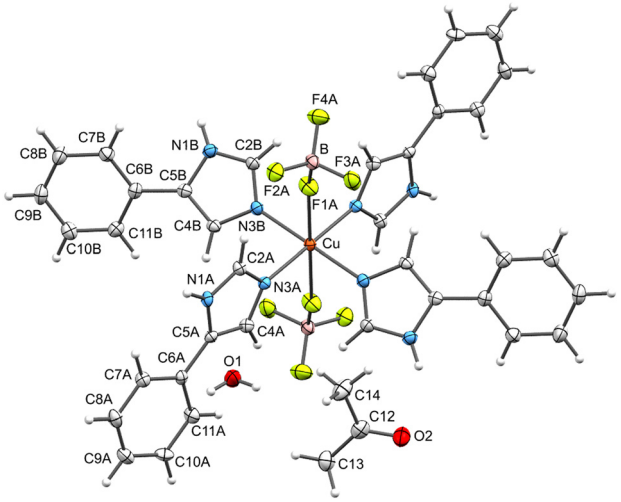

Fig. 1 View of the structure of solvatomorph **1**·2Me_2CO·2H_2O. Displacement ellipsoids are drawn at the 50% probability level. Atoms generated by symmetry through the inversion centre located on the copper ion are not labelled. Only the major-occupancy disorder components of the BF_4^- ions are shown.

The X-ray structure determination of all compounds (**1**–**19**) revealed that the initially used 4-phenylimidazole ligand (HL) is present as its 5-phenylimidazole tautomeric form. This rearrangement, termed as annular tautomerism of 4(5)-phenylimidazole,[65–67] is a result of the amphoteric character of the imidazole and involves the exchange of a proton from the pyrrole-type atom N1 to the pyridine-type atom N3. Tautomerism is accompanied by a significant change in ligand conformation and it is thus likely that the 5-phenyl form of the HL ligand is the most favourable one in terms of the formation of these complexes.

Compounds **1**–**17** crystallize in the $P\bar{1}$ space group, with the exception of **1**·2Me_2CO·2H_2O crystallizing in $P2_1/c$ (Table 1). The asymmetric unit of these compounds, except for **8**·1.33(*tert*-BuOH), contains half a $[Cu(BF_4)_2(HL)_4]$ host molecule (Z' = 1/2), with the copper(II) atom situated on an inversion centre. In **8**·1.33(*tert*-BuOH) there are one and a half host molecules in the asymmetric unit (Z' = 3/4), in which one of the two symmetry-independent copper(II) atoms is in a general position (Cu1) and the second one (Cu2) on an inversion centre. As previously mentioned, the isolated crystalline product **18**, $[Cu(HL)_4(MeCN)(H_2O)_{0.4}](BF_4)_2$, using CH_2Cl_2/MeCN as solvents, is not the expected solvatomorph; however it has been included in the study for comparison purposes. It has molecular symmetry, with a C_2 axis passing through the N_{MeCN}–Cu–O_{H_2O} direction of the complex (Z' = 1/2) and crystallizes in the *Pnn*2 space group (Fig. S2a†). The replacement of the BF_4^- ligands with $\{SiF_2O(OMe)\}^-$ coordinated ions in the solvatomorph **19**·0.8$MeNO_2$ has an impact on its molecular and crystal symmetry (Fig. S3†): the complex lacks molecular symmetry and crystallizes in the *P*2/*n* space group. The coordination geometry in all complexes (**1**–**19**) is distorted octahedral: this involves the pyridine-type nitrogen atom from the four ligands in the equatorial positions; in the axial positions there are two fluorine atoms from the terminal BF_4^- ions (**1**–**17**), or one O_{H_2O} and one N_{MeCN} atom (**18**), or two O atoms from the monodentate $\{SiF_2O(OMe)\}^-$ ions (**19**). The Cu^{II} – $F_{BF_4^-}$ bonds in **1**–**17** are weak (2.44–2.55 Å) and the metal centre is in an axially elongated octahedral environment (4 + 2); this is a consequence of the Jahn-Teller effect, typical for $3d^9$ systems. BF_4^- was traditionally considered as a typical example of a 'noncoordinating ion' 40 years ago or so. However, with the advent of single-crystal X-ray crystallography, it became evident that this anion can also be coordinated. To account for the coordination of this complex anion (and other anions such as $CF_3SO_3^-$, ClO_4^-, AlX_4^-, MF_6^- with X = Cl, Br, I; M = P, As, Sb, *etc.*), the term 'weakly coordinating anion' (WCA) was coined.[51] This expression allows for weak coordination, but also includes the potential of such complexes to serve as precursors of the 'noncoordinated' cation, for example, in catalytic processes. Thus, in complexes **1**–**17**, the BF_4^- ion can be best described as WCA.

The bond lengths and angles observed for the current complexes are similar (*e.g.* the Cu^{II}–N_{HL} bond lengths range from 1.99 to 2.02 Å). To compare the conformation of the $[Cu(BF_4)_2(HL)_4]$ molecules in compounds **1**–**17**, the relative orientation of the imidazole rings within each complex, as well as the orientation of the phenyl ring relative to the imidazole ring for each HL ligand are reported in Table 2. It appears that the conformation of the complexes is similar, with variations that presumably help to minimize steric hindrance, facilitate the effective formation of intermolecular synthons, and accommodate the included solvents.

Table 2 The dihedral angles (°) between the least-squares calculated planes through the atoms of the imidazole and phenyl rings of the $[Cu(BF_4)_2(HL)_4]$ molecules for solvatomorphs **1**–**17**[a]

Compound	ImA/ImB	ImA/PhRA	ImB/PhRB
1	66.1(1)	8.0(1)	26.4(1)
2	81.0(1)	12.0(2)	23.4(1)
3	80.6(2)	13.9(2)	27.8(2)
4	88.3(1)	16.7(1)	14.3(1)
5	79.5(2)	4.1(3)	4.4(3)/41.0(3)/34.3(3)[b]
6	88.2(2)	18.5(2)	18.4(3)
7	82.1(1)	16.4(2)	7.9(2)/26.7(2)[b]
8[c]	86.5(1)	7.9(1)	21.7(3)
9	82.4(1)	6.8(1)	15.1(1)
10	73.8(1)	2.6(2)	22.4(1)
11[d]	81.3(5)/79.9(5)	11.6(4)	29.5(7)/20.1(7)
12	83.4(1)	13.4(2)	25.6(2)
13	84.4(3)	4.3(3)	21.5(8)/48.9(8)[b]
14	80.2(2)	17.0(2)	31.5(2)
15	79.7(1)	17.4(1)	23.4(3)/44.2(3)[b]
16	83.0(3)	29.8(4)	15.7(3)
17	84.1(1)	28.3(1)	17.7(1)

[a] ImA: imidazole ring N1A–C2A–N3A–C4A–C5A; ImB: imidazole ring N1B–C2B–N3B–C4B–C5B; PhRA: phenyl ring C6A–C7A–C8A–C9A–C10A–C11A; PhRB: C6B–C7B–C8B–C9B–C10B–C11B. [b] Values for all orientations of the disordered phenyl ring PhRB. [c] For comparison with the HL ligands of the other structures, only the centrosymmetric $[Cu(BF_4)_2(HL)_4]$ molecule of **8**·1.33(*tert*-BuOH) is reported. [d] Values for the two orientations B and C of the disordered ligand B.

 This journal is © The Royal Society of Chemistry 2024

Open Access Article. Published on 07 June 2024. Downloaded on 7/31/2025 6:43:31 AM. This article is licensed under a Creative Commons Attribution 3.0 Unported Licence.

Considering the similarities in the unit-cell dimensions, the same space group ($P\bar{1}$) and Z′ (= 1/2) and the similar internal arrangement in the related crystal lattices [in this instance, the conformation of the $Cu(BF_4)_2(HL)_4$ host molecules], compounds **1**–**17** (with the exception of **1** and **8**) could be described as isostructural solvatomorphs.[68,69] However, the different hydrogen-bonding capabilities of the solvent molecules lead to variations in the networks of intermolecular interactions formed (see below).

The geometrical parameters of the strong H-bonding motifs for all compounds are given in Table 3. The supramolecular structures of the compounds are sorted and studied into three groups based on the type of solvent they contain (polar protic, polar aprotic and non-polar) and the resulting hydrogen-bonding patterns (synthons).

The supramolecular patterns of a molecule in its crystalline environment are visualized by the 3D molecular Hirshfeld surface, defined by the molecule *and* the proximity of its nearest neighbours, and therefore encode information about all its intermolecular interactions.[70–72] In addition, the accompanying 2D fingerprint plots provide information for the relative contribution of the various types of interactions on the Hirshfeld surfaces. Hirshfeld surfaces and associated fingerprints for three representative structures with different solvent type, **6**·2(1-BuOH) with polar protic solvent, **10**·2DMF with polar aprotic solvent and **17**·(*n*-hexane) with non-polar solvent, along with detailed description, are given in Fig. S4.†

i) Polar protic solvents: compounds 1–9. The solvents included in these compounds are H_2O+Me_2CO (**1**), MeOH (**2**), EtOH (**3**), 1-PrOH (**4**), 2-PrOH (**5**), 1-BuOH (**6**), iso-BuOH (**7**), *tert*-BuOH (**8**) and 1-PeOH (**9**) and (except Me_2CO) have an effective donor–acceptor capability. The mixture of water and acetone is considered as a polar protic solvent, because of the presence of the former. The $[Cu(BF_4)_2(HL)_4]$ molecules also feature classical hydrogen-bond donors (the imidazole N–H group) and acceptors (the tetrafluoroborate fluorine atoms). Therefore, these groups are expected to be involved in solute-solvent hydrogen-bonding packing patterns in the solid state. Analysis of the crystal structures of the isostructural compounds **2**–**7** and **9** shows that they all have the same packing organization. The molecules are assembled in 1D tapes by intermolecular N1A–H1A···F2 patterns along the *b* axis and by N1B–H1B···$O_{solvent}$–H···F3 patterns along the *a* axis (Fig. 2). These cross-linked tapes along *a* and *b* form rigid 2D layers parallel to the *ab* plane of the unit cell, with the solvents and two of the four ligands of the complexes protruding on either side of the layers. In the latter motif along *a*, the alcohol solvents act as both donors and acceptors bridging neighboring molecules and, apparently, as spacers, allowing the HL ligands to acquire the proper conformation to form these motifs. For example, for compound **2**·2MeOH, the distance N1A···F2A is 2.683(4) Å, and the distance N1B···F3A is 4.378(4) Å. As shown in Table 1, the increasing molecular size of the included alcohols is accompanied by a gradual increase of the unit cell parameters and the corresponding volumes. However, this

Table 3 Geometry (Å, °) of the strong hydrogen-bonding motifs in compounds **1**–**19**[a]

D–H···A	D–H	H···A	D···A	<(DHA)
1·2Me_2CO·2H_2O				
N1A–H1A···F2A^{i}	0.88(2)	1.93(2)	2.796(10)	166(2)
N1B–H1B···O1^{i}	0.86(2)	1.92(2)	2.777(3)	173(3)
O1–H1···F3A^{ii}	0.81(2)	2.03(2)	2.832(5)	168(3)
O1–H2···O2^{iii}	0.84(2)	1.94(2)	2.776(3)	174(3)
2·2MeOH				
N1A–H1A···F2A^{iv}	0.85(2)	1.91(2)	2.683(4)	152(3)
N1B–H1B···O1^{v}	0.85(2)	1.95(2)	2.804(3)	177(3)
O1–H1···F3A^{vi}	0.85(2)	1.90(3)	2.705(9)	158(4)
3·2EtOH				
N1A–H1A···F2A^{iv}	0.86(2)	1.93(3)	2.722(6)	151(5)
N1B–H1B···O1	0.86(2)	1.96(3)	2.798(6)	165(6)
O1–H1···F3A^{vii}	0.86(2)	1.90(1)	2.671(8)	148(4)
4·2(1-PrOH)				
N1A–H1A···F2^{iv}	0.85(2)	1.91(2)	2.749(2)	168(3)
N1B–H1B···O1^{v}	0.86(2)	1.96(2)	2.812(2)	173(3)
O1–H1···F3^{vi}	0.83(3)	1.95(3)	2.775(2)	173(3)
5·1.4(2-PrOH)				
N1A–H1A···F2A^{viii}	0.85(5)	2.03(6)	2.757(11)	143(6)
N1B–H1B···O1^{vii}	0.86(4)	1.86(5)	2.721(11)	176(9)
O1–H1···F3A	0.82(5)	1.79(5)	2.586(12)	163(5)
6·2(1-BuOH)				
N1A–H1A···F2^{ix}	0.85(2)	1.93(3)	2.754(5)	161(5)
N1B–H1B···O1^{vii}	0.86(2)	1.93(2)	2.773(5)	168(5)
O1–H1···F3	0.84(2)	1.97(3)	2.767(5)	159(6)
7·2(iso-BuOH)				
N1A–H1A···F2A^{iv}	0.84(2)	1.97(2)	2.812(7)	176(3)
N1B–H1B···OA1^{vii}	0.83(2)	2.10(2)	2.925(10)	172(4)
OA1–HA1···F3A	0.84(2)	1.99(4)	2.790(9)	160(9)
8·1.33(*tert*-BuOH)				
N1A–H1A···F10^{x}	0.85(2)	2.05(2)	2.805(3)	148(3)
N1B–H1B···F2^{xi}	0.85(2)	2.00(2)	2.820(3)	163(3)
N1C–H1C···O1^{xii}	0.83(2)	1.97(2)	2.778(4)	163(4)
N1D–H1D···O2	0.86(2)	1.96(2)	2.811(4)	168(3)
N1E–H1E···F6	0.85(2)	1.91(2)	2.741(3)	164(3)
N1F–H1F···F3^{xiii}	0.85(2)	2.04(2)	2.857(3)	161(3)
O1–H1···F11^{xiv}	0.84(2)	2.01(2)	2.841(3)	170(4)
O2–H2···F7^{ix}	0.84(2)	2.08(3)	2.844(3)	150(4)
9·2(1-PeOH)				
N1A–H1A···F2^{viii}	0.85(2)	2.01(2)	2.818(2)	159(2)
N1B–H1B···O1^{vii}	0.85(2)	1.92(2)	2.755(2)	164(2)
O1–H1···F3	0.80(2)	2.01(2)	2.806(2)	171(3)
10·2DMF				
N1A–H1A···F2A^{xi}	0.84(2)	1.95(2)	2.786(7)	169(3)
N1B–H1B···O1^{xii}	0.84(2)	1.96(2)	2.776(3)	164(2)
11·1.2Me_2CO				
N1A–H1A···F2A^{xv}	0.85(2)	2.07(5)	2.832(7)	149(7)
N1B–H1B···O1	0.86(2)	2.03(1)	2.839(2)	157(6)
N1C–H1C···F3B^{vii}	0.86(2)	2.00(4)	2.855(2)	172(2)
12·2THF				
N1A–H1A···F2^{xii}	0.85(2)	2.12(2)	2.965(3)	171(3)
N1B–H1B···OA^{xvi}	0.85(2)	1.95(2)	2.778(7)	164(4)
13·1.85(1,4-dioxane)				
N1A–H1A···F2A^{iv}	0.85(2)	2.02(4)	2.823(1)	156(7)
N1B–H1B···O1	0.85(2)	2.06(4)	2.840(1)	153(8)
14·0.86EtOAc				
N1A–H1A···F2^{ix}	0.84(2)	1.97(2)	2.768(4)	157(4)
N1B–H1B···F3^{vii}	0.84(2)	2.14(3)	2.869(4)	146(4)
15·Et_2O				
N1A–H1A···F2^{xi}	0.84(2)	1.96(2)	2.754(3)	157(3)
N1B–H1B···F3^{vii}	0.85(2)	2.13(2)	2.866(3)	144(2)
16·0.7DIPE				
N1A–H1A···F2^{xii}	0.86(2)	2.06(4)	2.862(7)	155(7)
N1B–H1B···F3^{viii}	0.86(2)	2.00(4)	2.782(6)	150(7)
17·(*n*-hexane)				
N1A–H1A···F2^{xvii}	0.85(2)	2.11(2)	2.876(3)	149(3)

Open Access Article. Published on 07 June 2024. Downloaded on 7/31/2025 6:43:31 AM.
This article is licensed under a Creative Commons Attribution 3.0 Unported Licence.

Table 3 *(continued)*

D–H···A	D–H	H···A	D···A	<(DHA)
N1B–H1B···F3^{xviii}	0.84(2)	1.98(2)	2.770(3)	155(3)
18				
N1A–H1A···F1^{xix}	0.87(3)	1.99(3)	2.825(6)	161(6)
N1B–H1B···F2^{xx}	0.86(3)	1.96(3)	2.792(5)	161(5)
O1–H1···F3	0.85(2)	1.57(2)	2.414(9)	179(9)
19·0.8MeNO$_2$				
N1A–H1A···F4^{xxi}	0.86(2)	1.94(3)	2.719(5)	150(4)
N1B–H1B···F2^{xxii}	0.86(2)	1.87(2)	2.686(5)	158(4)
N1C–H1C···F3A^{iv}	0.86(2)	1.98(2)	2.828(5)	168(4)
N1D–H1D···F1	0.86(2)	1.98(2)	2.828(4)	169(4)

[a] For the disordered fluorine atoms of the BF_4^- ions, only the hydrogen-bonding of the major-occupancy disorder components is shown. Symmetry codes: (i) $x, y, 1+z$; (ii) $-1+x, y, -1+z$; (iii) $x, 1/2-y, -1/2+z$; (iv) $x, -1+y, z$; (v) $1+x, y, 1+z$; (vi) $x, y, -1+z$; (vii) $1+x, y, z$; (viii) $x, 1+y, z$; (ix) $1-x, 1-y, 1-z$; (x) $-x, -y, -z$; (xi) $1-x, 2-y, 1-z$; (xii) $-1+x, y, z$; (xiii) $-x, 1-y, -z$; (xiv) $1+x, 1+y, z$; (xv) $-x, -y, 1-z$; (xvi) $x, -1+y, -1+z$; (xvii) $2-x, 1-y, 1-z$; (xviii) $1-x, -y, 1-z$; (xix) $1/2-x, 1/2+y, 1/2-z$; (xx) $1/2+x, 3/2-y, 1/2-z$; (xxi) $3/2-x, y, 3/2-z$; (xxii) $5/2-x, y, 3/2-z$.

trend is not evident in compounds **4**·2(1-PrOH) and **5**·1.4(2-PrOH), probably due to the different shapes of the two isomer solvents or the partial occupancy of 2-PrOH in the crystal lattice.

The molecular self-assembly in the hydrated compound **1**·2Me_2CO·2H_2O (Fig. 1) is directed by the same type of hydrogen-bonding patterns as in compounds **2**–**7** and **9**, forming 2D layers parallel to the *ac* plane of the unit cell (Table 3). In addition, the second H-atom of the water molecule, which is not involved in this pattern, forms a strong O_w–H···$O_{acetone}$ interaction with a lattice acetone solvent molecule. It appears that the above presented $P\bar{1}$ crystal lattice of the isostructural compounds **2**–**7** and **9** can no longer accommodate the additional acetone molecule, and eventually **1**·2Me_2CO·2H_2O crystallizes in the $P2_1/c$ space group.

Compound **8**·1.33(*tert*-BuOH), in $P\bar{1}$ with 1.5 $[Cu(BF_4)_2(HL)_4]$ molecules in the asymmetric unit, seems more complicated. Nevertheless, the molecules are similarly linked *via* N–H···F and N–H···$O_{tert\text{-}BuOH}$–H···F patterns forming rigid 2D layers parallel to the $(10\bar{1})$ plane of the unit cell with the solvents and two of the four ligands of each complex lying on either side of the layers.

In all **1**–**9** structures, all hydrogen-bond donor and acceptor groups of the molecules and solvents are fully engaged in hydrogen-bonding motifs (see Table 3). When not hindered by steric effects or the prevailing stronger patterns, some weak π···π interactions between the aromatic rings of the ligands in the layers and between adjacent layers, along with a few non-classic C–H···F/O and C–H···π interactions, are also observed and help to stabilize the structures (Fig. S4†).

ii) Polar aprotic solvents: compounds 10–13. The solvents included in these compounds are DMF (**10**), Me_2CO (**11**), THF (**12**), and 1,4-dioxane (**13**), featuring only hydrogen-bond acceptors. The $[Cu(BF_4)_2(HL)_4]$ molecules in all compounds are assembled in 1D tapes by intermolecular N1A–H1A···F2 patterns along the *b* axis (or along *a* in **12**·2THF), a pattern also encountered in compounds **1**–**9** (see Fig. 3 for the structure of **12**·2THF). Their solvents are also hydrogen-bonded to the second donor group of the complexes forming N1B–H1B···$O_{solvent}$ interactions (Fig. S4†). The structures are further extended according to the particular features of each structure and solvent. In solvatomorphs **10** and **12**, the 1D tapes are connected in 2D layers [parallel to the (222) plane in **10** and the *ab* plane in **12**] *via* weak π···π contacts and their 3D structures are completed through weak C–H···π and C–H···F interactions. In solvatomorph **11** (Fig. S5†), the positional disorder of a HL ligand (orientations B and C) and the partial occupancy of the acetone solvent allow this ligand

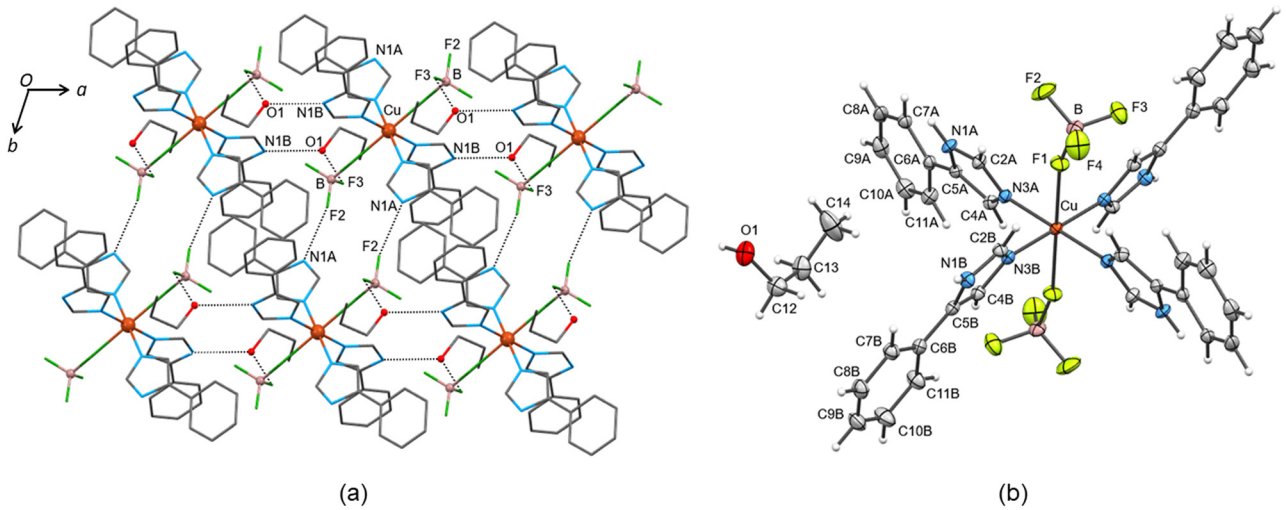

Fig. 2 The structure of solvatomorph **4**·2(1-PrOH). (a) View of a 2D layer parallel to the *ab* plane organized by N1B–H1B···$O1_{(1\text{-}PrOH)}$–H···F3 motifs along the *a* axis and N1A–H1A···F2 motifs along the *b* axis. (b) The molecular structure of **4**·2(1-PrOH). Displacement ellipsoids are drawn at the 50% probability level. Atoms generated by symmetry through the inversion centre located on the copper(II) ion are not labelled.

 This journal is © The Royal Society of Chemistry 2024

Open Access Article. Published on 07 June 2024. Downloaded on 7/31/2025 6:43:31 AM.
This article is licensed under a Creative Commons Attribution 3.0 Unported Licence.

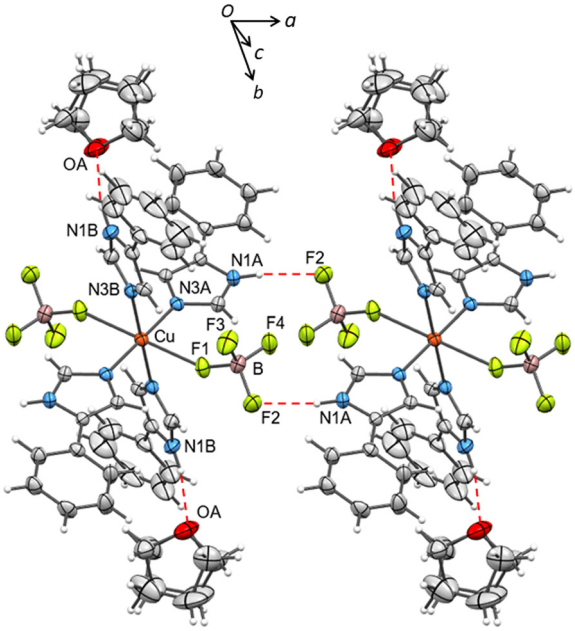

Fig. 3 View of a 1D tape in the crystal packing of **12**·2THF formed by intermolecular N1A–H1A···F2 patterns along the *a* axis (shown in red dashed lines). Both orientations of the disordered THF solvent molecules are shown. Displacement ellipsoids are drawn at the 50% probability level. Only selected atoms have been labelled.

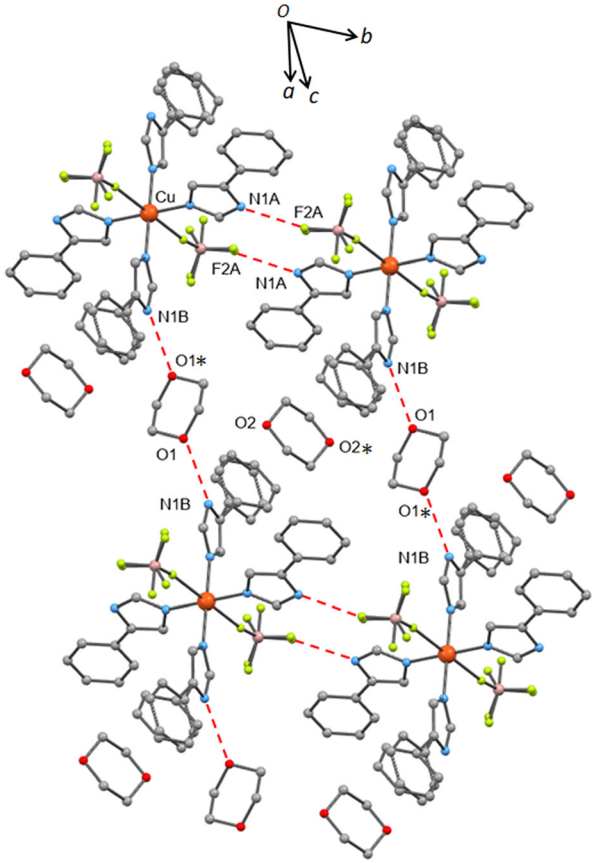

Fig. 4 View of a 2D layer of solvatomorph **13**·1.85(1,4-dioxane). The layer is organized by strong synthons shown in red dashed lines. Both orientations of the disordered phenyl rings of a HL ligand and the BF_4^- ions are shown. Only selected atoms have been labelled.

to participate, in addition to the described N1B–H1B···$O1_{acetone}$ interaction, in a second one (N1C–H1C···F3B) forming 1D tapes along the *a* axis. Weak π···π, C–H···π and C–H···F interactions contribute in stabilizing its 3D structure (Fig. S5†). The asymmetric unit in compound **13**, contains two halves of centrosymmetric 1,4-dioxane solvent molecules (Fig. 4). The first solvent bridges, through its centrosymmetrically-related oxygen atoms O1 and O1*, two neighboring $[Cu(BF_4)_2(HL)_4]$ molecules in the [101] direction: N1B–H1B···O1–//–O1*···H1B–N1B. This interaction together with N1A–H1A···F2A along the *b* axis form a compact 2D structure parallel with the $(10\bar{1})$ plane. Some π···π interactions and other weak contacts between these layers organize the 3D assembly of the structure. The second 1,4-dioxane molecule (O2) is not involved in any major bonding pattern, except for two weak C–H···O interactions with the first dioxane molecule on either side.

iii) Non-polar solvents: compounds 14–17. The solvents included in these compounds are EtOAc (**14**), Et_2O (**15**), DIPE (**16**), and *n*-hexane (**17**). The solvatomorph **14** with ethyl acetate has been included in this category; ethyl acetate is commonly referred to as a non-polar to weak polar aprotic solvent. Analysis of the crystal structures of these compounds shows that they all have the same packing organization. Due to the inability of the included solvents to participate in strong hydrogen-bonding patterns with the HL ligands (as in all previous structures), the $[Cu(BF_4)_2(HL)_4]$ molecules are oriented to form directly hydrogen-bonding motifs with each other. As shown in Table 3 and Fig. 5, intermolecular N1A–H1A···F2 and N1B–H1B···F3 interactions link the molecules into tapes along the *a* and *b* axes forming 2D layers parallel with the *ab* plane, whereas the solvents and two of the four phenyl rings of the ligands are located on either side of the layers. A few weak π···π and C–H···π contacts are also observed within the layers of the structures. Weak π···π or/and C–H···π contacts between the aromatic rings of adjacent layers contribute to the structure extension and stabilization in 3D. A visualization of the intermolecular interactions in compound **17**·(*n*-hexane) is shown in Fig. S4.† Practically, the solvents only form few and very weak interactions, without any structural implications, with the rest of the structures, *i.e.* C–H···O (**14**) and C–H···F (**14**, **15** and **17**). The solvent atoms in these compounds have rather elongated thermal ellipsoids; this is probably due to the lack of significant interactions with the rest of their structure.

Compounds 18 and 19·0.8MeNO$_2$. Although the structure of $[Cu(HL)_4(MeCN)(H_2O)_{0.4}](BF_4)_2$ (**18**) (Fig. S2a†) differs from the solvatomorphs **1–17**, the presence of the same hydrogen-bond donor and acceptor groups results in the formation of the same supramolecular synthons (N–H···F and O_{water}–H···F, Table 3). Each BF_4^- counterion links three surrounding $[Cu(HL)_4(MeCN)(H_2O)_{0.4}]$ molecules leading to the assembly of a robust 3D structure in the *Pnn*2 space group (Fig. S2b†).

Open Access Article. Published on 07 June 2024. Downloaded on 7/31/2025 6:43:31 AM.
This article is licensed under a Creative Commons Attribution 3.0 Unported Licence.

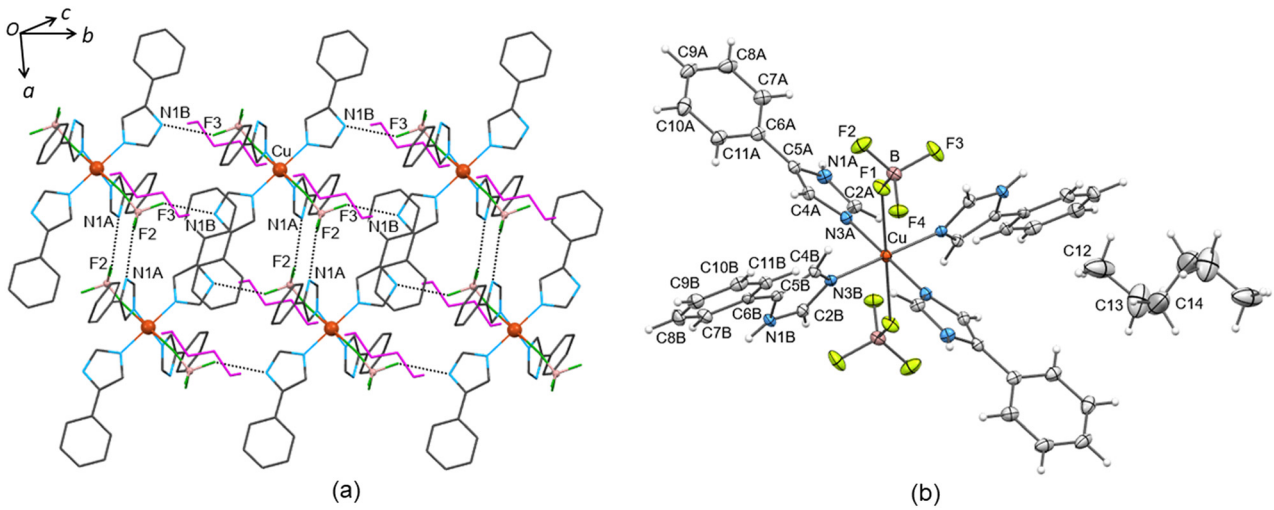

Fig. 5 The structure of solvatomorph **17**·(*n*-hexane). (a) View of a 2D layer parallel to the *ab* plane organized by N1A–H1A···F2 motifs along the *a* axis and N1B–H1B···F3 motifs along the *b* axis. The *n*-hexane solvents are drawn in magenta colour. (b) The molecular structure of **17**·(*n*-hexane). Displacement ellipsoids are drawn at the 50% probability level. Atoms generated by symmetry through the inversion centre located on the copper(II) ion are not labelled.

Some π···π contacts complement the intermolecular organization. Similarly, the N–H···F synthons are also the driving force in the molecular self-assembly of compound $[Cu\{SiF_2O(OMe)\}_2(HL)_4]\cdot 0.8MeNO_2$ (**19**·0.8$MeNO_2$), Fig. S3b.† The packing resembles that of compounds **14**–**17** and the structure crystallizes in the *P*2/*n* space group. The molecules are linked by N–H···F interactions forming 2D layers parallel with the *ab* plane, with the nitromethane solvents and two of the four phenyl rings of the ligands located on either side of the layers. Some weak C–H···O and C–H···F contacts between the nitromethane solvents and ligands of neighboring layers are also observed.

Location and role of the solvents in the crystal structures. Examination of the crystal structures of the 17 solvatomorphs shows that the solvents are located in channels (in most cases) or lattice pockets[73] (Fig. 6). The void space, calculated by PLATON as V_{void}/V_{cell} (%) after the removal of the solvent molecules, ranges from 16.0% to 30.1% (Table 4); similar values are obtained using the VOIDS option in Mercury software. Compounds **18** and **19**·0.8$MeNO_2$ are also included for comparison. The difference observed in compounds **4**·2(1-PrOH) and **5**·1.4(2-PrOH), 25.0% and 20.9%, respectively, could possibly be related to the difference in solvent shape; however, the phenyl ring close to the 2-PrOH solvent is triply disordered and only the major-occupancy conformer of this ring was retained in the calculations. As reported, the structure of **8**·1.33(*tert*-BuOH) is different (Z = 3) from the other isomers **6**·2(1-BuOH) and **7**·2(iso-BuOH) and the *tert*-BuOH solvents are pairwise encapsulated in lattice pockets (Fig. S6†). The structure of **13**·1.85(1,4-dioxane) contains two half 1,4-dioxane molecules in the asymmetric unit lying on inversion centres and arranged alternately in channels along the *b* axis (Fig. 7). All four non-polar solvents in compounds **14**–**17** (EtOAc, Et_2O, DIPE and *n*-hexane, respectively) are located on inversion centres. Thus, the ratio of the $[Cu(BF_4)_2(HL)_4]$ host molecule to the included solvent is reduced to 1 : 1, contrary to 1 : 2 (or 1 : 1.33 in **8**) observed in the preceding structures. The 1 : 2 ratios are dictated by the need to fully exploit all strong hydrogen-bond donor and acceptor groups, whereas in compounds **14**–**17** this is not necessary because the solvents are not engaged in any strong hydrogen-bonding pattern. In addition, the placement of the solvents on inversion centres helps to reduce the relative volume (%) they occupy within the unit cell and to accommodate them efficiently, considering they are large and elongated in shape. There is no solvent included in the crystal structure of **18** but only BF_4^- counterions located in lattice pockets (Fig. S7†); likewise, the nitromethane solvent in **19**·0.8$MeNO_2$ is also located in lattice pockets.

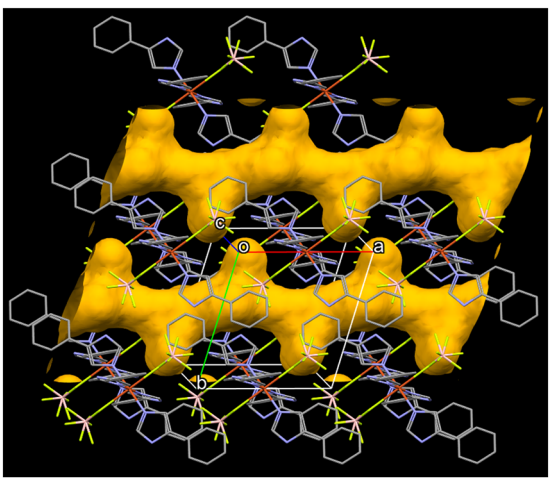

Fig. 6 View of the 3D structure of solvatomorph **2**·2MeOH showing the channels (in yellow) along the *a* axis that contain the MeOH solvent molecules. The hydrogen atoms have been omitted. The channels were drawn using MERCURY.

 This journal is © The Royal Society of Chemistry 2024

Open Access Article. Published on 07 June 2024. Downloaded on 7/31/2025 6:43:31 AM. This article is licensed under a Creative Commons Attribution 3.0 Unported Licence.

Table 4 Void space and location of solvents in the compounds of this study

Compound[a]	V_{void}/V_{cell} (%)	SG[b] (Z)[c]	Void space of solvents or counterions (for **18**)
1·2Me_2CO·2H_2O	25.4	$P2_1/c$ (2)	Channels along c
2·2MeOH	17.5	$P\bar{1}$ (1)	Channels along a
3·2EtOH	17.6	$P\bar{1}$ (1)	Channels along a
4·2(1-PrOH)	25.0	$P\bar{1}$ (1)	Channels along a
5·1.4(2-PrOH)[d]	20.9	$P\bar{1}$ (1)	Channels along [1$\bar{1}$0]
6·2(1-BuOH)	26.2	$P\bar{1}$ (1)	Channels along a
7·2(iso-BuOH)[d]	25.3	$P\bar{1}$ (1)	Channels along a
8·1.33(*tert*-BuOH)	19.6	$P\bar{1}$ (3)	Lattice pockets
9·2(1-PeOH)	30.1	$P\bar{1}$ (1)	Channels along a
10·2DMF	26.9	$P\bar{1}$ (1)	Channels along a
11·1.2Me_2CO[d]	16.3	$P\bar{1}$ (1)	Lattice pockets
12·2THF	24.9	$P\bar{1}$ (1)	Channels along a
13·1.85(1,4-dioxane)	20.8	$P\bar{1}$ (1)	Channels along b
14·0.86EtOAc	19.1	$P\bar{1}$ (1)	Channels along a
15·Et_2O	16.0	$P\bar{1}$ (1)	Channels along a
16·0.7DIPE	21.6	$P\bar{1}$ (1)	Channels along a
17·(*n*-hexane)	20.2	$P\bar{1}$ (1)	Channels along a
18	10.9	$Pnn2$ (2)	Lattice pockets (BF_4^-)
19·0.8$MeNO_2$	9.5	$P2/n$ (4)	Lattice pockets

[a] **1** to **17**: $[Cu(BF_4)_2(HL)_4]$. [b] SG: space group. [c] Z: number of molecules in the unit cell. [d] Only the major-occupancy conformer of a disordered phenyl ring close to the solvent is used in the calculations.

IR study and TGA data in brief

The selected IR wavenumbers for the complexes cited in the Experimental Section refer to crushed, freshly isolated crystals; for this reason, the spectra exhibit bands of the lattice solvents. The presence of H-bonded H_2O or alcohol lattice molecules in **1–9** is proven by the appearance of a medium-to-strong intensity band at ~3400 cm^{-1} assigned to the ν(OH) mode; the broadness of the band is indicative of the participation of the –OH groups in H-bonds. This band is absent, as expected, from the spectra of **10–19**, with the exception of **18**; the spectrum of the latter shows a weak broad band assigned to ν(OH) of the coordinated H_2O molecule.[74] The bands at ~1675 (**1**, **11**), 1650 (**10**) and 1701 cm^{-1} (**14**) can be safely assigned to the characteristic ν(C=O) mode of the carbonyl (**1**, **11**), amide (**10**) and ester (**14**) functionalities that are present in the lattice solvents of the complexes. The ν(C≡N) mode of the coordinated MeCN is hardly seen in the spectrum of **18**, while the medium-intensity bands at 1561 and 1376 cm^{-1} in the spectrum of **19** are attributed to the $\nu_{as}(NO_2)$ and $\nu_s(NO_2)$, respectively, vibrations of the lattice $MeNO_2$.[75] A common weak to medium, broad feature in the spectra of all the complexes is due to the ν(NH) mode of the 5-phenylimidazole ligands, the broadness again indicating the participation of the N–H group in H bonds.

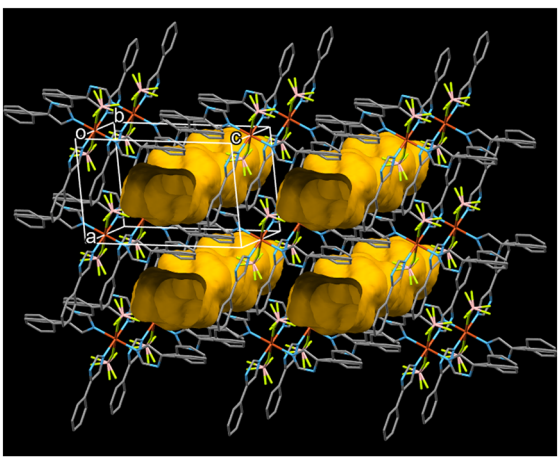

Fig. 7 View of the 3D structure of solvatomorph **13**·1.85(1,4-dioxane) showing the channels (in yellow) along the b axis that contain the 1,4-dioxane solvent molecules. The hydrogen atoms have been omitted. The channels were drawn using MERCURY.

The band at 1026 cm^{-1} in the spectrum of **19** is assigned[74] to the ν(Si–F) mode of the tetrahedral $SiF_2O(OMe)^-$ ligand. The presence of tetrafluoroborato ligands (**1–17**) and BF_4^- counterions (**18**) is manifested by the appearance of the characteristic ν(BF) and δ(FBF) bands. The four normal modes of vibration of the 'free', *i.e.* uncoordinated (T_d) BF_4^- ion are the $\nu_1(A_1)$ [ν_s(BF)], $\nu_2(E)$ [δ_d(FBF)], $\nu_3(F_2)$ [ν_d(BF)] and $\nu_4(F_2)$ [δ_d(FBF)] ones;[74] only ν_3 and ν_4 are IR-active. Monodentate coordination of the BF_4^- group (as in **1–17**) lowers the symmetry from T_d to C_{3v}, splitting each of the triply degenerate modes, ν_3 and ν_4, into two components ($F_2 \rightarrow A_1 + E$). The previously IR-inactive modes, ν_1 and ν_2, are activated in this process, *i.e.* monodentate coordination.[74–76] Common bands due to the BF_4^- ligands in **1–17** appear at ~1070, ~1040, ~760 and 515 cm^{-1}, the first and the third ones probably overlapping with HL vibrations since they also appear in the spectrum of free 4-phenylimidazole. We tentatively assign the three high-wavenumber bands to the $A_1 + E$ components of ν_3 and to the activated ν_1 mode (exact assignments would be risky), and the band at ~515 cm^{-1}

Open Access Article. Published on 07 June 2024. Downloaded on 7/31/2025 6:43:31 AM. This article is licensed under a Creative Commons Attribution 3.0 Unported Licence.

arising from the splitting of ν_3 and/or from the activated ν_2 mode.[77] All these spectral characteristics reveal a lower symmetry of the BF_4^- ion due to monodentate coordination. However, none of compounds **1–17** exhibits all six vibrations corresponding to the C_{3v} symmetry. This is probably due to the masking of the additional expected bands by ligand's vibrations; however, this feature has also been explained[52,77] in terms of the WCA behaviour of BF_4^-. Somewhat to our surprise, the four BF_4^- bands appear also in the spectrum of **18** although this complex contains purely ionic (T_d) tetrafluoroborate counterions. This might be due to the involvement of the anions in H bonds, which makes BF_4^- to spectroscopically behave as 'pseudocoordinated'.

Thermogravimetric (TG) data are available for complexes **2–5**, **7**, **10**, **12**, **15** and **17** (Fig. S8†). The samples were in the form of crushed (powdered) crystals and thus they were not completely dried, but contained various amounts of lattice solvents. For this reason, an in-depth discussion is not possible. The samples lose the lattice solvents at low temperatures, mainly dependent on their boiling point. Thus, the removal of MeOH in **2**·2MeOH is complete at ~70 °C, whereas that of DMF in **10**·2DMF is complete at ~190 °C. The observed experimental trend might be a coincidence since it is known that boiling point is a bulk property while this is not the case for single crystals that include lattice solvents. Thermally stable intermediates are clearly visible at temperatures above those of the complete loss of lattice solvents, corresponding to the unsolvated compounds. The main decomposition of the complexes occurs at ~300 °C and is rather similar for most samples. For **3**·2EtOH, **10**·2DMF, **12**·2THF and **15**·Et_2O decomposition gradually continues above 800 °C, the highest temperature limit of the instrument used. For the other complexes, a final plateau appears at slightly below or slightly above 600 °C and approximate mass loss calculations indicate that the final residue is CuO. For example, the final residue in **17**·(*n*-hexane) is 10.1% of the original mass, while the theoretical value for CuO is 8.9%. The small discrepancies observed in most cases are presumably due to the assumption that the original samples at 20 °C contained all the amount of the lattice solvent found through crystallography.

Conclusions

The Cu(II)/HL/BF_4^- reaction system shows a remarkable competence to form solvatomorphs. The complexes are crystallized as solvated forms from a large number of polar protic, polar aprotic and non-polar solvents. The solvents included are H_2O + Me_2CO (**1**), MeOH (**2**), EtOH (**3**), 1-PrOH (**4**), 2-PrOH (**5**), 1-BuOH (**6**), iso-BuOH (**7**), *tert*-BuOH (**8**), 1-PeOH (**9**), DMF (**10**), Me_2CO (**11**), THF (**12**), 1,4-dioxane (**13**), EtOAc (**14**), Et_2O (**15**), DIPE (**16**) and *n*-hexane (**17**). They all crystallize in the $P\bar{1}$ space group with $Z = 1$, except **1**·2Me_2-CO·2H_2O (in $P2_1/c$, Z = 2) and **8**·1.33(*tert*-BuOH) (in $P\bar{1}$, $Z = 3$). The initially used 4-phenylimidazole ligand is present in all complexes as its 5-phenylimidazole tautomeric form. There are two solvent molecules per $[Cu(BF_4)_2(HL)_4]$ unit (with full or partial site occupancy due to disorder), except for solvatomorphs **1**·2Me_2CO·2H_2O, **8**·1.33(*tert*-BuOH) and **14–17** (in which the solvents are located on inversion centres, presumably to fit more efficiently in the unit cell since they are large and elongated). The $[Cu(BF_4)_2(HL)_4]$ host molecules in the solvatomorphs have similar conformations with a few minor differences in the orientation of the aromatic rings, most likely to facilitate the formation of the H-bonding synthons and accommodate the included solvents. All solvent molecules reside in channels, except for compounds **8**·1.33(*tert*-BuOH) and **11**·1.2Me_2CO (with a highly disordered HL ligand) in which the solvents are found in lattice pockets. The void space of the channels (or lattice pockets), calculated after the removal of the solvent molecules, ranges from 16.0% to 30.1% of the unit-cell volume. It follows that the $[Cu(BF_4)_2(HL)_4]$ host framework of the seventeen structures can readily incorporate solvent molecules containing two to six light non-H atoms (C, O, N).

At the supramolecular level, the large number of the solvatomorphs with a variety of solvents (with respect to their H-bond functionalities, size and shape) allows for interesting conclusions to be drawn. The molecular self-assembly is clearly directed by robust synthons formed by the N–H/BF_4^- donor/acceptor groups of the $[Cu(BF_4)_2(HL)_4]$ host molecules. Depending on the H-bond capabilities of the solvents included three distinct cases show up: i) the polar protic solvents (compounds **1–9**) participate in the formation of N–H···$O_{solvent}$–H···F motifs and, together with the other N–H···F synthons, lead to compact 2D layers; ii) the polar aprotic solvents (compounds **10–13**) are, perforce, only terminally linked through N–H···$O_{solvent}$ interactions and, thus, the remaining N–H/BF_4^- groups can only form 1D tapes *via* N–H···F synthons; however, 1,4-dioxane (**13**), due to its centrosymmetrically-related oxygen atoms O and O*, is an exception participating in N–H···O–//–O1*···H–N motifs, which together with the other N–H··F interactions form 2D layers; and iii) the non-polar solvents (compounds **14–17**) are not engaged in any strong H-bonding motif and the N–H/BF_4^- groups form directly 2D layers *via* N–H···F synthons. In all three cases the 1D or 2D constructions are further stabilized in 3D by means of weak interactions (*e.g.* π···π/C–H···π/C–H···O/C–H···F). All the N–H and O–H donor groups of the ligands and the solvents, respectively, and most of the fluorine acceptor atoms of the BF_4^- ions are engaged in synthon formation in the course of the crystallization process. Finally, the packing organization of the 'failed' structures **18** and **19**·0.8$MeNO_2$, corroborates the structure-directing role of the robust N–H···F synthon conserved among all seventeen solvatomorphs studied.

It seems that in the present series of solvatomorphs, the solvents have a distinct role in the formation of self-assembled structures, either by interfering with the otherwise expected synthon by forming alternative associations, or by connecting terminally to donor groups of the guest molecule, or by simply residing in channels participating only in structurally non-important weak interactions.

 This journal is © The Royal Society of Chemistry 2024

Open Access Article. Published on 07 June 2024. Downloaded on 7/31/2025 6:43:31 AM. This article is licensed under a Creative Commons Attribution 3.0 Unported Licence.

Work currently in progress in our laboratory involves the synthetic and structural study of the related Cu(II)/HL/ClO_4^-, Cu(II)/HL/PF_6^-, Cu(II)/HL/$CF_3SO_3^-$ and Cu(II)/HL/SiF_6^{2-} systems in order to study the effect of solvatomorphism as a function of the weakly coordinating anion, and the extensions of this type of chemistry in other, non-Jahn–Teller distorted divalent metals, *e.g.* Mn(II), Co(II), Ni(II) and Zn(II).

Author contributions

MD: synthesis, X-ray structure analysis, IR/microanalyses, writing; NP, CP, AT: data collection/X-ray crystallography/TGA; DP: mechanistic studies, writing; VN, SPP: conceptualization, supervision, data curation, writing/draft preparation, project administration.

Conflicts of interest

There are no conflicts to declare.

Acknowledgements

We thank Dr A. Kitos for some help with the crystallization experiments.

Notes and references

1 P. Klitou, C. M. Pask, L. Onoufriadi, I. Rosbottom and E. Simone, *Cryst. Growth Des.*, 2020, **20**, 6573.
2 U. J. Griesser, in *Polymorphism in the Pharmaceutical Industry: The Importance of Solvates*, ed. R. Hilfiker, Wiley-VCH, Weinheim, 2006, pp. 211–233.
3 H. G. Brittain, *J. Pharm. Sci.*, 2012, **101**, 464.
4 B. T. Ibragimov, *CrystEngComm*, 2007, **9**, 111.
5 T. L. Threlfall, *Analyst*, 1995, **120**, 2435.
6 A. Nangia and G. R. Desiraju, *Chem. Commun.*, 1999, 605.
7 K. R. Seddon, *Cryst. Growth Des.*, 2004, **4**, 1087.
8 G. R. Desiraju, *Cryst. Growth Des.*, 2004, **4**, 1089.
9 J. Bernstein, *Cryst. Growth Des.*, 2005, **5**, 1661.
10 J. Bernstein, *Cryst. Growth Des.*, 2011, **11**, 632.
11 A. Nangia, *Cryst. Growth Des.*, 2006, **6**, 2.
12 B. Stöger, P. Kautny, D. Lumpi, E. Zobetz and J. Fröhlich, *Acta Crystallogr., Sect. B: Struct. Sci.*, 2012, **68**, 667.
13 M. du Plessis and L. J. Barbour, *Dalton Trans.*, 2012, **41**, 3895.
14 M. K. Stanton and A. Bak, *Cryst. Growth Des.*, 2008, **8**, 3856.
15 J. A. R. P. Sarma and G. R. Desiraju, in *Crystal Engineering: The Design and Application of Functional Solids*, ed. K. R. Seddon and M. J. Zaworotko, Kluwer, Dordrecht, 1999, vol. 539, pp. 325–356.
16 A. Nangia and G. R. Desiraju, *Angew. Chem., Int. Ed.*, 2019, **58**, 4100.
17 S. Ranjan, R. Devarapalli, S. Kundu, S. Saha, S. Deolka, V. Vangala and C. Reddy, *IUCrJ*, 2020, **7**, 173.
18 G. R. Desiraju, *IUCrJ*, 2017, **4**, 710.
19 C. H. Görbitz and H.-P. Hersleth, *Acta Crystallogr., Sect. B: Struct. Sci.*, 2000, **56**, 526.
20 X. Hao, S. Parkin and C. P. Brock, *Acta Crystallogr., Sect. B: Struct. Sci.*, 2005, **B61**, 689.
21 R. Mondal and J. A. K. Howard, *CrystEngComm*, 2005, **7**, 462.
22 M. Köppen, V. Meyer, J. Ångström, K. Inge and N. Stock, *Cryst. Growth Des.*, 2018, **18**, 4060.
23 R. Seetharaj, P. V. Vandana, P. Arya and A. S. Mathew, *Arabian J. Chem.*, 2019, **12**, 295.
24 M. Yamada, Z. Shen and M. Miyake, *Chem. Commun.*, 2006, 2569.
25 A. Bernard, K. Zhang, D. Larson, K. Tabatabaei and S. M. Kauzlarich, *Inorg. Chem.*, 2018, **57**, 5299.
26 K. A. Kounavi, C. Papatriantafyllopoulou, A. Tasiopoulos, S. P. Perlepes and V. Nastopoulos, *Polyhedron*, 2009, **28**, 3349.
27 K. A. Kounavi, M. J. Manos, E. Moushi, C. Papatriantafyllopoulou, A. Tasiopoulos and V. Nastopoulos, *Cryst. Growth Des.*, 2012, **12**, 429.
28 K. A. Kounavi, E. Moushi, M. J. Manos, C. Papatriantafyllopoulou, A. Tasiopoulos and V. Nastopoulos, *CrystEngComm*, 2012, **14**, 6492.
29 K. A. Kounavi, A. Kitos, E. Moushi, M. J. Manos, C. Papatriantafyllopoulou, A. Tasiopoulos, S. P. Perlepes and V. Nastopoulos, *CrystEngComm*, 2015, **17**, 7510.
30 A. Kitos, E. Moushi, M. J. Manos, C. Papatriantafyllopoulou, A. Tasiopoulos, S. P. Perlepes and V. Nastopoulos, *CrystEngComm*, 2016, **18**, 4733.
31 V. Duros, C. Papatriantafyllopoulou, A. Kitos, A. Tasiopoulos and V. Nastopoulos, *Acta Crystallogr., Sect. B: Struct. Sci., Cryst. Eng. Mater.*, 2019, **75**, 599.
32 D. Reinen, *Comments Inorg. Chem.*, 1983, **2**, 227.
33 F. A. Cotton, G. Wilkinson, C. A. Murillo and M. Bochmann, *Advanced Inorganic Chemistry*, Wiley, New York, 6th edn, 1999, pp. 865.
34 E. C. Constable, *Metals and Ligand Reactivity: An Introduction to the Organic Chemistry of Metal Complexes*, VCH, Weinheim, 1996, pp. 240–245.
35 S.-S. Chen, *CrystEngComm*, 2016, **18**, 6543.
36 S. J. Lippard and J. M. Berg, *Principles of Bioinorganic Chemistry*, University Science Books, Mill Valley, California, 1994.
37 R. M. Roat-Malone, *Bioinorganic Chemistry*, Wiley, New Jersey, 2002.
38 G. R. Desiraju, *Angew. Chem., Int. Ed. Engl.*, 1995, **34**, 2311.
39 J. W. Steed and J. L. Atwood, *Supramolecular Chemistry*, Wiley, Chichester, 1st edn, 2009.
40 G. M. J. Schmidt, *Pure Appl. Chem.*, 1971, **27**, 647.
41 T. Steiner, *Angew. Chem., Int. Ed.*, 2002, **41**, 48.
42 C. B. Aakeröy, N. R. Champness and C. Janiak, *CrystEngComm*, 2010, **12**, 22.
43 J. D. Dunitz and A. Gavezzotti, *Cryst. Growth Des.*, 2012, **12**, 5873.
44 C. A. Hunter and J. K. M. Sanders, *J. Am. Chem. Soc.*, 1990, **112**, 5525.
45 C. Janiak, *J. Chem. Soc., Dalton Trans.*, 2000, 3885.
46 M. Nishio, Y. Umezawa, H. Suezawa and S. Tsuboyama, in *The importance of pi-Interactions in Crystal Engineering: Frontiers in Crystal Engineering*, ed. E. R. T. Tiekink and J. Zukerman-Schpector, Wiley, Singapore, 2012, pp. 1–31.

Open Access Article. Published on 07 June 2024. Downloaded on 7/31/2025 6:43:31 AM.
This article is licensed under a Creative Commons Attribution 3.0 Unported Licence.

47 J. Lozada, W. X. Lin, R. M. Cao-Shen, R. A. Tai and D. M. Perrin, *Angew. Chem.*, 2023, **62**, e202215371.
48 R. I. Petrikat and S. Becker, *Z. Anorg. Allg. Chem.*, 2022, **648**, e202200150.
49 J. Reedijk, *Comments Inorg. Chem.*, 1982, **1**, 379.
50 W. Beck and K. Sünkel, *Chem. Rev.*, 1988, **88**, 1405.
51 I. Krossing and I. Raabe, *Angew. Chem., Int. Ed.*, 2004, **43**, 2066.
52 J. Burt, W. Grantham, W. Levason, M. E. Light and G. Reid, *Polyhedron*, 2015, **85**, 530.
53 *CrysAlis PRO (version 1.171.38.43)*, Rigaku Oxford Diffraction, Yarnton, UK, 2015.
54 A. Altomare, G. Cascarano, C. Giacovazzo, A. Guagliardi, M. C. Burla, G. Polidori and M. Camalli, *J. Appl. Crystallogr.*, 1994, **27**, 435.
55 G. M. Sheldrick, *Acta Crystallogr., Sect. A: Found. Adv.*, 2015, **71**, 3.
56 L. Palatinus and G. Chapuis, *J. Appl. Crystallogr.*, 2007, **40**, 786.
57 L. Palatinus, S. J. Prathapa and S. van Smaalen, *J. Appl. Crystallogr.*, 2012, **45**, 575.
58 G. M. Sheldrick, *Acta Crystallogr., Sect. C: Struct. Chem.*, 2015, **71**, 3.
59 A. L. Spek, *Acta Crystallogr., Sect. D: Biol. Crystallogr.*, 2009, **65**, 148.
60 O. V. Dolomanov, L. J. Bourhis, R. J. Gildea, J. A. K. Howard and H. Puschmann, *J. Appl. Crystallogr.*, 2009, **42**, 339.
61 L. J. Farrugia, *J. Appl. Crystallogr.*, 2012, **45**, 849.
62 C. F. Macrae, I. Sovago, S. J. Cottrell, P. T. A. Galek, P. McCabe, E. Pidcock, M. Platings, G. P. Shields, J. S. Stevens, M. Towler and P. A. Wood, *J. Appl. Crystallogr.*, 2020, **53**, 226.
63 D. H. Kim, S. J. Kwak, J. H. Jeong, S. You, S. K. Nam, Y. Kim and W. B. Lee, *ACS Omega*, 2021, **6**, 16009.
64 H. Díaz-Salazar, J. C. Rodríguez-Colín, J. Vazquez-Chavez and M. Hernández-Rodríguez, *J. Org. Chem.*, 2023, **88**, 8150.
65 R. M. Claramunt, M. D. Santa María, L. Infantes, F. H. Cano and J. Elguero, *J. Chem. Soc., Perkin Trans. 2*, 2002, **2**, 564.
66 M. Kubicki, *Acta Crystallogr., Sect. B: Struct. Sci.*, 2004, **60**, 191.
67 M. E. García-Rubiño, D. Choquesillo-Lazarte, M. C. Núñez and J. M. Campos, *Acta Crystallogr., Sect. C: Cryst. Struct. Commun.*, 2011, **67**, o484.
68 P. Bombicz, N. V. May, D. Fegyverneki, A. Saranchimega and L. Bereczki, *CrystEngComm*, 2020, **22**, 7193.
69 P. Bombicz, *IUCrJ*, 2024, **11**, 3.
70 M. A. Spackman and J. J. McKinnon, *CrystEngComm*, 2002, **4**, 378.
71 M. A. Spackman and D. Jayatilaka, *CrystEngComm*, 2009, **11**, 19.
72 P. R. Spackman, M. J. Turner, J. J. McKinnon, S. K. Wolff, D. J. Grimwood, D. Jayatilaka and M. A. Spackman, *J. Appl. Crystallogr.*, 2021, **54**, 1006.
73 J. F. Gallagher and P. Mocilac, *J. Mol. Struct.*, 2021, **1234**, 130149.
74 K. Nakamoto, *Infrared and Raman Spectra of Inorganic and Coordination Compounds*, Wiley, New York, 4th edn, 1986, pp. 130–141, 228–233, 280–282.
75 C. Stamou, W. Papawassiliou, J. P. Carvalho, K. F. Konidaris, V. Bekiari, P. Dechambenoit, A. J. Pell and S. P. Perlepes, *Inorg. Chem.*, 2021, **60**, 4889.
76 A. P. Gaughan, Jr., Z. Dori and J. A. Ibers, *Inorg. Chem.*, 1974, **13**, 1657.
77 A. N. Chebotarev, M. V. Shestakova and T. M. Shcherbakova, *Russ. J. Coord. Chem.*, 2002, **28**, 131.

 This journal is © The Royal Society of Chemistry 2024